8-6-2011

Crashworthiness optimization of vehicle structures considering the effects of lightweight material substitution and dummy models

Andrew Eric Parrish

CRASHWORTHINESS OPTIMIZATION OF VEHICLE STRUCTURES CONSIDERING THE EFFECTS OF LIGHTWEIGHT MATERIAL SUBSTITUTION AND DUMMY MODELS

By

Andrew Eric Parrish

A Thesis
Submitted to the Faculty of
Mississippi State University
in Partial Fulfillment of the Requirements
for the Degree of Master of Science
in Aerospace Engineering
in the Department of Aerospace Engineering

Mississippi State, Mississippi

August 2011

CRASHWORTHINESS OPTIMIZATION OF VEHICLE STRUCTURES

CONSIDERING THE EFFECTS OF LIGHTWEIGHT MATERIAL

SUBSTITUTION AND DUMMY MODELS

By

Andrew Eric Parrish

Approved:

Masoud Rais-Rohani Professor of Aerospace Engineering (Director of Thesis)	Mark F. Horstemeyer Professor of Mechanical Engineering (Committee Member)
Esteban Marin Research Professor Center for Advanced Vehicular Systems (Committee Member)	J. Mark Janus Associate Professor of Aerospace Engineering Graduate Coordinator of Department of Aerospace Engineering
Sarah A. Rajala Dean of Bagley College of Engineering	

Name: Andrew Eric Parrish

Date of Degree: August 6, 2011

Institution: Mississippi State University

Major Field: Aerospace Engineering

Major Professor: Masoud Rais-Rohani

Title of Study: CRASHWORTHINESS OPTIMIZATION OF VEHICLE STRUCTURES CONSIDERING THE EFFECTS OF LIGHTWEIGHT MATERIAL SUBSTITUTION AND DUMMY MODELS

Pages in this Study: 89

Candidate for Degree of Master of Science

This study uses numerical design optimization with advanced metamodeling techniques to investigate the effects of material substitution and dummy models on crashworthiness characteristics of automotive structures. A full-scale Dodge Neon LS-DYNA finite element model is used in all structural analysis and optimization calculations. Optimization is performed using vehicle-based responses for multiple crash scenarios and occupant-based responses for one crash scenario. An AZ31 magnesium alloy is substituted for the baseline steel in twenty-two vehicle parts. Five base metamodels and an Optimized Ensemble metamodel are used to develop global surrogate models of crash-induced responses. Magnesium alloy is found to maintain or improve vehicle crashworthiness with an approximate 50% reduction in selected part mass using vehicle-based responses while dummy-based designs show less percentage decrease in weight. Vehicle-based responses selected to approximate dummy injury metrics do not show the same relative change compared to dummy-based responses.

ACKNOWLEDGMENTS

The author thanks his advisor Dr. Masoud Rais-Rohani for his guidance and assistance while completing this work and Cynthia Tamasco and Ali Najafi for their assistance.

The author acknowledges that this material is based on the work supported by the US Department of Energy under Award Number DE-EE0002323.

TABLE OF CONTENTS

LIST OF TABLES

LIST OF FIGURES

CHAPTER I

INTRODUCTION

Stricter automotive regulations on fuel economy and growing concerns for emissions have created challenges for design engineers. Some motivations for improving fuel economy are to save money filling up the gas tank, reduce carbon dioxide emissions, reduce oil dependence, and increase energy sustainability. This study considers only structural approaches to meeting these demands and does not consider improvements to other aspects of vehicle design such as the engine.

One way of improving fuel economy is by reducing vehicle weight. This can be accomplished using substitution of lighter weight materials, optimization of existing designs, or a combination of the two. Fuel savings, however, should not come at a cost of occupant safety in a crash situation. See Figure 1.1, this study explores this problem by

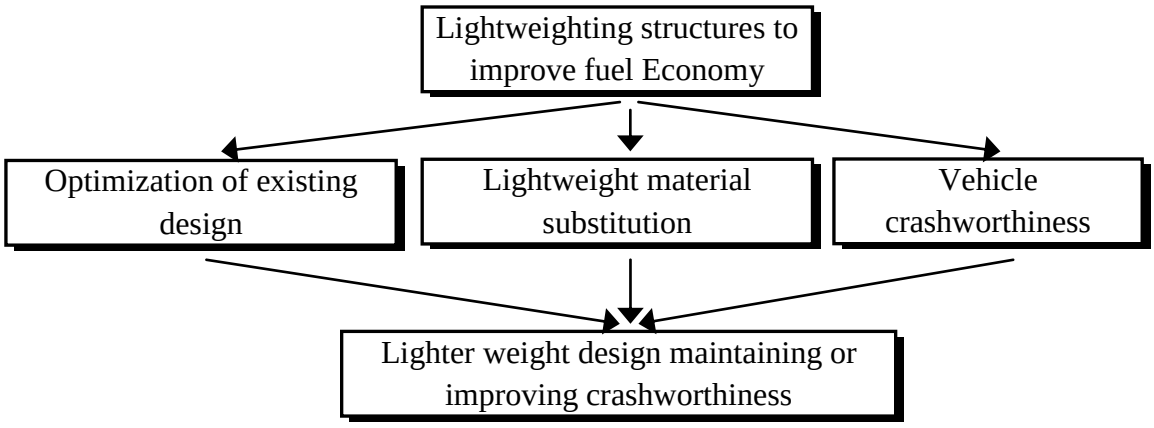

Figure 1.1 Considerations for a Lighter Weight Design

combining design optimization techniques and material substitutions to reduce vehicle weight while maintaining the vehicles crash performance or its crashworthiness.

Lightweight Magnesium Alloys

The U.S. Department of Energy has sponsored many studies in the area of Automotive Lightweighting Materials[1] under the Vehicle Technologies Program. This effort investigates the application of lightweight materials such as magnesium alloys and improvements in structural design and manufacturing for lightweighting of vehicle structures. "Magnesium Vision 2020: A North American Automotive Strategic Vision for Magnesium"[2] proposes strategies for researching and incorporating more magnesium alloy parts into automobile design. It says magnesium is a good candidate material to replace steel due to magnesium's high strength-to-weight ratio, fewer parts due to larger castings, and the ability to tune magnesium parts to frequencies related to Noise, Vibration, and Harshness (NVH). Magnesium, however, requires more research to address corrosion and manufacturing issues as well as brittle fracture at high strain rates before it is ready for widespread use.

Design Optimization

Design optimization is another method that can be used to reduce vehicle weight by improving the existing design. Design optimization uses mathematical techniques to find values of the design variables that maximize or minimize an objective or merit function without violating any of the specified design constraints. These techniques require a number of function evaluations to search for the optimum design. The general

optimization problem in this study is one that minimizes weight while maintaining or improving crashworthiness relative to the baseline or initial design.

Three methods of structure lightweighting optimization are shape, sizing, and topology optimization. Shape optimization manipulates the geometric shape of a component such as changing angles, the length of a section, or introducing a completely new geometry. Sizing optimization keeps the geometry but changes the size of a part. Part thickness or gauge of selected parts is often used as a design variable in automobile sizing optimization. Topology optimization finds the best distribution of material within a given part for given boundary conditions. This method adds material to key areas and removes material from non-critical areas resulting in a part that has an optimal mass distribution within the specified domain.

Akkerman et al.[3] used shape and sizing optimization to improve crashworthiness of an automotive instrument panel. Rais-Rohani et al.[4] used shape and sizing optimization to improve crashworthiness of a vehicle by altering the geometry of the side rails. Strategies for topology optimization can be found in Jung and Gea[5], Mozumder et al.[6], and Rouhi and Rais-Rohani[7].

This study uses a sizing optimization approach. The full-scale, finite element vehicle model used as the test bed in this study has components with complicated geometries making shape optimization challenging. The components in this model are shell elements which makes thickness changes simple. Choosing thicknesses as design variables for crashworthiness optimization studies is widely used in the literature [4, 6, 8-11].

Crashworthiness

Crashworthiness is the ability of the structure to protect occupants during crashes. Performing real crash tests to obtain necessary data for crashworthiness optimization is not feasible. Finite element (FE) crash simulations are used in place of physical experiments to obtain responses needed for optimization or exploratory studies. Finite element analysis (FEA) separates a computer model of the component(s) into nodes connected by elements. Nodal interactions and positions are followed during simulations such as crash. One FEA code frequently used for crash simulations is LS-DYNA developed by Livermore Software Technology Corporation. LS-DYNA is used in this study to perform nonlinear transient dynamic explicit FEA of full-scale vehicle crashes for crashworthiness simulations and optimization.

Objective and constraint responses for crashworthiness optimization are often selected to measure or estimate the likelihood of occupant injury. The US Department of Transportation places requirements on crash responses felt by crash test dummies through the Federal Motor Vehicle Safety Standards (FMVSS)[12]. The FMVSS specify upper limits on responses such as chest deflection, upper leg axial force, neck moment, neck force, rib deflection, and Head Injury Criteria (HIC). Some of these limits are used as responses for design optimization in Chapter V. FMVSS contain specifics for multiple crash scenarios as well as for different classes of vehicles. Some crash scenarios in these requirements are Full Frontal Impact (FFI), Offset Frontal Impact (OFI), Side Impact (SIDE), Roll-over or roof impact, and rear impact.

Obtaining these values in FE simulations requires a crash occupant model set correctly in the vehicle model. This includes interior models of the car and can include

airbags and seatbelt models. One type of FE occupant model uses metallic, rubber, and plastic materials to simulate the dummies used in laboratory crash tests to rate new vehicles. Noureddine et al.[13] present work developing and validating a FE dummy model called a Hybrid III dummy model. Hybrid III models can be used in multiple crash scenarios but are usually not used for side impact scenarios. A crash test dummy specifically designed for side impacts is used in these cases.

Research has been progressing in recent years on FE models that simulate a human occupant rather than a crash test dummy. These models attempt to create a model with materials that accurately model human tissue and bone. Silvestri and Ray[14] developed an FE model of a knee, thigh, and hip including ligaments. Components of their model were developed using material characteristics from laboratory test results of bones and ligaments in the model region.

Alternative responses must be chosen if an FE model with an occupant model is not available. Internal energy absorption, intrusion distance, and acceleration measured at selected locations are used as substitutes. These responses focus on the vehicle's crash performance rather than occupant injury metrics. Fang et al.[8] used internal energy absorption of selected components at two time steps along with peak engine top acceleration. Liao et al.[10] used a combination of occupant-based responses and vehicle based responses including an integration of the deceleration curve and intrusion distance at the toeboard. Intrusion distance of the front panel for frontal impacts and intrusion distance of the door for side impacts were considered by Fang et al.[9]. Horstemeyer et al.[15] compared optimum designs using energy-based and injury-based designs and found that the injury-based design was safer than the energy-based design.

A number of multi-objective problems have been solved regarding crashworthiness. One study improved crash performance while maintaining weight in a Full Frontal Impact (FFI)[8] and another improved crash performance considering multiple impact scenarios[9]. Another study solved a two-step optimization problem minimizing weight and vehicle crash responses before optimizing the occupant restraint system based on occupant injury criteria[10].

Metamodels

Simulation runtime is a major obstacle in optimization studies. In many cases, hundreds or thousands of function evaluations may be required for solving a design optimization problem depending on the method selected as well as the numbers of design variables and constraints used. This problem is trivial when an analytical function is used to describe the objective and constraints but poses a big challenge when high fidelity FE crash simulations are required to obtain these values. A single crash simulation in this study takes between one and a half to five hours depending on the crash scenario using 4 six core Intel X5660 with 48GB of total RAM. Another important consideration is the non-smooth (noisy) behavior of some of the crash responses that could pose problems in application of gradient-based optimization methods. Hence, approximate mathematical models or metamodels are often used to overcome the difficulties associated with computational cost and noisy responses.

Metamodels are surrogate models that approximate function values and are widely used in automotive crashworthiness studies [8-11] to provide approximate responses at a design point. Responses predicted using a metamodel will have some error associated with them when compared to simulation or test results at the same design point.

Metamodels can also provide an analytical function for a response depending on the specific metamodeling techniques used.

A metamodel is built using data sets obtained through FE simulations or physical tests at the training points defined by the selected design of experiments (DOE) model. DOE uses mathematical algorithms to create a populated design space where points are distributed throughout the domain. Two DOE types frequently used for crashworthiness optimization are Taguchi orthogonal arrays[8,9] and Latin Hypercube Sampling (LHS)[10,16].

The number of training points used when building metamodels depends on a number of factors. These include the problem type, number of variables, metamodel type, and ease of obtaining results. The general agreement in the literature is that at least *3N* training points must be used where *N* is the number of design variables. Both Yang et al.[17], using an impact example, and Fang and Wang[18], using analytic benchmark problems, show that metamodels are generally more accurate as the number of training points increases but this trend is not true for some functions and metamodel types.

The next step to create an accurate metamodel is selecting the type to use. Different metamodeling techniques have been developed with different levels of complexity and accuracy. Turner[18] shows metamodels divided into three main groups. These groups are Geometric containing response surface models and spline-based models, Stochastic containing Kriging models and radial basis functions, and Heuristic containing kernel model, frequency domain methods and neural networks.

Metamodel comparison studies have been carried out by Jin et al.[20] and Wang et al.[21]. Both studies compared several metamodeling techniques using metrics such as accuracy, robustness, efficiency, transparency, flexibility, and conceptual simplicity for

benchmark as well as more industry relevant example problems. Results from studies such as these aided in the decision about which metamodeling techniques to use.

Additional contributing factors when selecting the techniques used here were popularity of the metamodeling method in automotive crashworthiness as well as availability of source code for the more complex models. Metamodel techniques explored in this study include Polynomial Response Surface (PRS), Radial Basis Function (RBF), Kriging (KR), Support Vector Regression (SVR), and Gaussian Process (GP). These choices cover all three categories discussed in Turner[19] and have strong or growing popularity. An optimized ensemble (ENS) of multiple metamodels as suggested by Acar and Rais-Rohani[22] is created using the five standalone models listed above. The ENS technique was used in Acar and Solanki[23] for a crashworthiness problem and shown to be more accurate than stand alone metamodels.

The degree of the polynomial in PRS as well as parameters in the formulations of RBF, KR, and SVR can be tuned to alter the predicted value and thus accuracy of the model. Tuning parameters, particularly for SVR, are crucial for an accurate metamodel. Stand alone metamodels for each response are developed and tuned for maximum accuracy before being used to construct an optimized ensemble of metamodels.

The thesis is organized as follows: Chapter II discusses the metamodels used to predict crash responses, Chapter III introduces the crash simulation FE models and responses, Chapter IV presents the optimization problems and results without the dummy model, Chapter V presents the optimization problem and results with the dummy model, and Chapter VI contains concluding remarks and future work.

CHAPTER II

METAMODELING TECHNIQUES

Metamodel construction begins with building a design of experiments (DOE) table, which represents a collection of design variable values at the selected training points that are spread throughout the design space. Design points for metamodels and in some cases test points come from the DOE. Design points or training points are used to fit the metamodel and test points are used to determine the accuracy of the model. A function response must be obtained at each of the DOE points by analytic function, simulation, or experiment. Metamodels can be built and tested for accuracy after the DOE and function values are obtained.

Polynomial Response Surface (PRS)

PRS is one of the most widely used and simplest metamodeling techniques, but it may not provide an accurate prediction for certain responses. The most typical form of PRS is a second-degree polynomial function of the form

$$\hat{f}(x) = b_o + \sum_{i=1}^{L} b_i x_i + \sum_{i=1}^{L} b_{ii} {x_i}^2 + \sum_{i=1}^{L-1} \sum_{j=i+1}^{L} b_{ij} x_i x_j \qquad (2.1)$$

where $\hat{f}(x)$ is the metamodel prediction at point x, L is the number of design variables in the design vector $\boldsymbol{x}$, and b_0, b_i, b_{ii}, b_{ij} are the unknown coefficients found using the least squares technique.

As a regression model, PRS does not pass through the training points. The degree of the polynomial can be changed or some of the terms appearing in Eq. (2.1) can be

omitted depending on the nonlinearity of the response function being modeled. The polynomial degree is treated as the tuning parameter for PRS.

Gaussian Process (GP)

Descriptions of Gaussian Process (GP) in this discussion follow that in Wang et al.[21] and Acar and Rais-Rohani[22]. The GP metamodel is a group of output variables $f_N = \{f_n(x_n^1, x_n^2, \dots, x_n^1)\}_{n=1}^N$ with a Gaussian joint probability distribution

$$P(f_N|C_N, X_N) = \frac{1}{\sqrt{(2\pi)^N |C_N|}} \exp\left[-\frac{1}{2}(f_N - \mu)^T {C_N}^{-1}(f_N - \mu)\right] \tag{2.2}$$

where $X_N \equiv \{x_n\}_{n=1}^N$ are N pairs of L-dimensional input variables $x_n = {x_n}^1, {x_n}^2, \dots, {x_n}^L$, C_N is the covariance matrix with elements of $C_{ij} = C(x_i, x_j)$, and μ is the mean output vector.

Elements of the covariance matrix C_N are calculated from

$$C_{ij} = \theta_1 exp\left[-\frac{1}{2}\sum_{l=1}^{L}\frac{\left(x_i^{(l)} - x_j^{(l)}\right)^2}{r_l^2}\right] + \theta_2 \tag{2.3}$$

$$C_{ij} = \theta_1 exp\left[-\frac{1}{2}\sum_{l=1}^{L}\frac{\left(x_i^{(l)} - x_j^{(l)}\right)^2}{r_l^2}\right] + \theta_2 + \delta_{ij}\theta_3 \tag{2.4}$$

where $\theta_1, \theta_2, \theta_3$, and $r_l$are referred to as "hyperparameters" with r_l being the length scale. θ_3 is an independent noise parameter and δ_{ij} is Kronecker's delta (equal to one when i = j and zero otherwise). These hyperparameters are selected to maximize logarithmic likelihood of the predictions matching the training data. This is given by

$$LL = -\frac{1}{2} log|C_N| - \frac{1}{2} {f_N}^T {C_N}^{-1} f_N - \frac{N}{2}\log(2\pi) + \ln\left(P(\theta)\right) \tag{2.5}$$

where $P(\theta)$is the prior distribution of the hyperparameters. This is usually uniform because no prior knowledge is available and can be equated to zero for optimization.

Eq. (2.3) and Eq. (2.4) define the interpolation and regression modes of the Gaussian process model, respectively. The former passes through all training points while the latter provides a smoother surface to help with noisy data. The prediction surface with noise filtered out is less complex and might not pass through all training points but this has better predictions at non-training points.

The response value at a prediction point $x_p = (x_p^1, x_p^2, \dots, x_p^L)$ is estimated as

$$\hat{f}(x_p) = k^T {C_N}^{-1} f_N \tag{2.6}$$

where $k = \left[C(x_1, x_p), \dots, C(x_N, x_p)\right]$. Standard deviation at the prediction point is available without requiring additional simulations or tests and can be calculated from

$$\sigma_{\hat{f}}(\boldsymbol{x}_p) = \kappa - k^T {C_N}^{-1} k \tag{2.7}$$

where $\kappa = C(x_p, x_p)$.

No tuning parameters are explored within GP. The MATLAB[24] toolbox from Rasmussen and Williams[25] is used to develop the GP metamodels.

Radial Basis Function (RBF)

This formulation of RBF requires normalized training and test points in the range of 0 to 1. This is done by dividing each variable by the maximum value of that variable in the DOE table. The basic form of RBF is given as

$$\hat{f}(x) = \sum_{i=1}^{N} \lambda_i \Phi(\|x - x_i\|) \tag{2.8}$$

where $\hat{f}(x)$ is the metamodel prediction at point *x*, *N* is the number of training points, *x* is the input vector of normalized variables, x_i is vector of normalized design variables at the *ith* training point, and $\|x - x_i\| = \sqrt{(x - x_i)^T (x - x_i)}$ is the Euclidean norm or distance *r* from point *x* to the training point x_i. The λ_i parameters are the unknown interpolation

coefficients that must be calculated. Φ is the radially symmetric basis function that can take on a number of forms. Eq. (2.8) represents a linear combination of a finite number of basis functions. Typical radial basis functions are listed below.

- Thin Plate Spline: $\Phi(r) = r^2 \ln(c * r)$
- Gaussian: $\Phi(r) = \exp(-c * r^2)$
- Multiquadric: $\Phi(r) = \sqrt{r^2 + c^2}$
- Inverse Multiquadric: $\Phi(r) = 1/\sqrt{r^2 + c^2}$

The value *c* is a constant that the user determines. Values of *r* are between 0 and 1 because the training and test points are between 0 and 1 resulting in $0 < c \leq 1$. In general, Multiquadric with *c* = 1 gives good results for many function types.

The interpolation coefficients, λ_i, can be found by minimizing the residual (the sum of the squares of the deviations) as

$$R = \sum_{j=1}^{N} \left[f(x_j) - \sum_{i=1}^{N} \lambda_i \Phi(\|\boldsymbol{x_j} - \boldsymbol{x_i}\|) \right]^2 \tag{2.9}$$

In matrix form, this is expressed as

$$[A]\{\lambda\} = \{f\} \tag{2.10}$$

where $[A] = \Phi(\|x_j - x_i\|)$ with *j=1,N*, and *i=1,N*. Solving Eq. (2.10) for λ and inputting into Eq. (2.8) generates predictions. Error analysis typically relies on data at test points outside of the training set since RBF is an interpolation model that passes through all the training points. The tuning parameters for RBF are Φ and *c*.

Kriging (KR)

Descriptions of Kriging follow those in Acar and Rais-Rohani[22], Lophaven et al.[26], and Simpson et al.[27]. For this discussion the design (training) point matrix is *s*, the corresponding training point function evaluations are *Y*, the test point or prediction point is *x*, and general variables *w* and *v* are introduced. This description of Kriging requires the training set to have zero mean and a covariance of 1. This is done by:

$$s = \frac{(s_{original} - \mu_s)}{\sigma_s} \tag{2.11}$$

$$Y = \frac{(Y_{original} - \mu_Y)}{\sigma_Y} \tag{2.12}$$

where *original* indicates the un-normalized values, μ_s and μ_Y are the means of the training points and their responses respectively, and σ_s and σ_Y are the standard deviations of the training points and their responses, respectively.

Kriging models assume the function takes the form of

$$\hat{f}(x) = \mathcal{P}(x) + Z(x) \tag{2.13}$$

where $\hat{f}(x)$ is the approximate function, $\mathcal{P}(x)$ is a polynomial function that globally approximates the actual function, and $Z(x)$ is the stochastic component that accounts for deviations or $Z(x) = r(x)^T * \hat{\gamma}$.

First, the polynomial portion of the model is explored, $\mathcal{P}(x)$. This is a linear combination of *np* polynomial functions, $p(x)$, and regression parameters $\hat{\beta}$:

$$\mathcal{P}(x) = p(x)^T * \hat{\beta} \tag{2.14}$$

The degree of the polynomial is chosen to be 0, 1, or 2 resulting in *np* polynomial equations, with a 1st degree polynomial generally being used. The 2nd degree (quadratic)

formulation is similar to the 2nd degree PRS model discussed previously. That is, with L = number of variables using general variable w:

$$\begin{gathered} degree\ 0(constant) \\ np = 1 \\ p_1(w) = 1 \end{gathered} \tag{2.15}$$

$$\begin{gathered} degree\ 1\ (linear) \\ np = L + 1 \\ p_1(w) = 1, p_2(w) = w_1, \dots, p_{L+1}(w) = w_L \end{gathered} \tag{2.16}$$

$$\begin{gathered} degree\ 2\ (quadratic) \\ np = \frac{1}{2}(L+1)(L+2) \\ p_1(w) = 1 \\ p_2(w) = w_1, \dots, p_{L+1}(w) = w_L \\ p_{L+2}(w) = {w_1}^2, \dots, p_{2L+1}(w) = w_1 w_L \\ p_{2L+2}(w) = {w_2}^2, \dots, p_{3L}(w) = w_2 w_L \\ \dots\ \dots\ p_{np}(w) = {w_{np}}^2 \end{gathered} \tag{2.17}$$

Polynomial function evaluations at each training point must be performed to fit the training data. Define *P(s)* or just *P* as:

$$P(s) = P = [p(s_1), \dots, p(s_N)]^T \tag{2.18}$$

where N is the number of training points. This is a vector of ones if the 0 degree polynomial is used.

The stochastic component Z allows the Kriging model to interpolate the response value and has a zero mean and covariance of

$$COV\left[Z(x_i), Z\left(x_j\right)\right] = \sigma^2 \mathcal{R}\left(\theta, x_i, x_j\right)\ i, j = 1, \dots, N \tag{2.19}$$

where σ^2 is the variance, $\boldsymbol{\mathcal{R}}\left(\theta, x_i, x_j\right)$ is the correlation function between sample points x_i and x_j and θ represents correlation parameters that must be calculated. The user defines the correlation function, $\boldsymbol{\mathcal{R}}\left(\theta, x_i, x_j\right)$, with a Gaussian correlation function generally chosen. Correlation functions use general variables w and v and are in the form

$$\mathcal{R}(\theta, w, v) = \prod_{k=1}^{L} \mathcal{R}_k(\theta_k, d_k) \tag{2.20}$$

where L is the number of design variables and $d_k = w_k - v_k$ is the distance between w_i and v_j at the *kth* component of the points. Some Kriging correlation functions are listed below:

- Gaussian: $\mathcal{R}_k(\theta_k, d_k) = \exp(-\theta_k {d_k}^2)$
- Exponential: $\mathcal{R}_k(\theta_k, d_k) = \exp(-\theta_k |d_k|)$
- Exp. General: $\mathcal{R}_k(\theta_k, d_k) = \exp(-\theta_k |d_k|^{\theta_{L+1}}), \quad 0 < \theta_{L+1} \leq 2$
- Linear: $\mathcal{R}_k(\theta_k, d_k) = max\{0, 1 - \theta_{L+1}|d_k|\}$
- Spherical: $\mathcal{R}_k(\theta_k, d_k) = 1 - 1.5{\xi_k}^2 + 0.5{\xi_k}^3, \quad \xi_k = min\{1, \theta_k|d_k|\}$
- Cubic: $\mathcal{R}_k(\theta_k, d_k) = 1 - 3{\xi_k}^2 + 2{\xi_k}^3, \quad \xi_k = min\{1, \theta_k|d_k|\}$
- Spline: $\mathcal{R}_k(\theta_k, d_k) = \varsigma(\xi_k), \quad \xi_k = \theta_k|d_k|$
  - $\varsigma(\xi_k) = \begin{Bmatrix} 1 - 15{\xi_k}^2 + 30{\xi_k}^3 & for\ 0 \leq \xi_k \leq 0.2 \\ 1.25(1 - \xi_k)^3 & for\ 0.2 < \xi_k < 1 \\ 0 & for\ \xi_k \geq 1 \end{Bmatrix}$

The correlation matrix *R(s)* or *R* is defined as

$$R(\theta, s) = R = \mathcal{R}(\theta, s_i, s_j),\ i, j = 1, \ldots, N \tag{2.21}$$

Maximum likelihood estimation is used to estimate the correlation parameter,θ. θ is found by solving the following optimization problem if a Gaussian correlation model is selected

$$min\ \psi(\theta) \equiv\ |R|^{1/N}\hat{\sigma}^2 \ \text{ or } \ \begin{matrix} \max \psi(\theta) = -[Nln(\hat{\sigma}^2) + ln|R|]/2 \\ s.t. \quad \theta > 0 \end{matrix} \tag{2.22}$$

where $|R|$ is the determinant of *R* and $\hat{\sigma}^2$ is the process variance defined as

$$\hat{\sigma}^2 = \left[\left(Y - P\hat{\beta}\right)^T R^{-1}(Y - P\hat{\beta})\right]/N \tag{2.23}$$

The initial value of θ as well as its upper and lower bounds influence the calculation of θ from Eq. (2.22) and the accuracy of the resulting Kriging model. θ usually falls between 0 and 2 with the initial value being taken as the midpoint. Almost any value of θ will produce a Kriging model and results will be predicted, but these predictions are not necessarily accurate. Solving the optimization problem in Eq. (2.22) will result in a more accurate Kriging model.

The steps to derive Eqs. (2.24) through (2.25) are not presented here, see Lophaven et al.[26] for a description of the derivation. Once regression and correlation functions are chosen, the response is predicted as

$$\hat{f}(x) = p(x)^T\hat{\beta} + r(x)^T\hat{\gamma} \tag{2.24}$$

where *p(x)* is the polynomial term found from Eq. (2.15) through Eq. (2.17), $r(x)$ is the correlation vector (see Eq. (2.25)), $\hat{\beta}$ comes from a generalized least squares solution and seen in Eq. (2.26), and $\hat{\gamma}$ is computed from the residual and seen in Eq. (2.27).

$$r(x) = [\mathcal{R}(\theta, s_1, x) \dots, \mathcal{R}(\theta, s_m, x)]^T \tag{2.25}$$

$$\hat{\beta} = (P^T R^{-1} P)^{-1} P^T R^{-1} Y \tag{2.26}$$

$$\hat{\gamma} = R^{-1}(Y - P\hat{\beta}) \tag{2.27}$$

Below are some key points about the discussion of Kriging.

1) $\hat{\beta}$ and $\hat{\gamma}$ are functions of training points (not test points). This means $\hat{\beta}$ and $\hat{\gamma}$ are constant for a given training set, so from Eq. (2.24) only the correlation and regression functions need to be evaluated at the test point(s) to get the Kriging prediction(s) once $\hat{\beta}$ and $\hat{\gamma}$ are found.
2) $\hat{\beta}$ and $\hat{\gamma}$ are functions of correlation parameter θ because $R(\theta, s)$

3) The quantity R^{-1} appears in multiple places. This can become very computationally expensive as the number training points (*N)* increases (*R* is an *N* by *N* matrix) which is common in a number of metamodeling applications. For this reason the inverse should be calculated using linear algebra techniques.
4) The best regression and correlation functions are dependent on the problem, but a 1st degree polynomial and a Gaussian correlation function serve as a good starting point.

The MATLAB toolbox developed in Lophaven et al.[26] is used in this study. The tuning parameters of KR explored are the polynomial degree, regression function, as well as the upper and lower bounds on θ.

Support Vector Regression (SVR)

Descriptions of SVR in this discussion follow that in Refs. (22, 28, 29, 30, 31). The literature suggests the design variables should be normalized to a range of [-1,1] or [0,1]. Simply, SVR constructs a hyperplane that passes near each design point such that they fall within a specified distance of the hyperplane. In two dimensions, this hyperplane is simply a line. The hyperplane is then used to predict other responses. SVR estimates the real function as

$$y = r(x) + \delta \tag{2.28}$$

where δ is an independent random noise, x is the multivariable input, y is the scalar output, and r is the mean of the conditional probability (regression function). See Cherkassky and Ma[28] and Gunn[29] for more information. SVR technique selects the "best"

approximate model from a group of selection models that minimize the prediction risk. Linear or nonlinear regression can be performed. When a linear regression is used, the pool of approximation models is given by

$$\hat{f}(x) = \langle \omega \cdot x \rangle + \mathrm{b} \tag{2.29}$$

where b is the bias term and $\langle \omega \cdot x \rangle$ is the dot product of ω and x. Minimizing empirical risk using the ε-insensitive loss function allows regression estimates. It is desirable to have a "flat" approximation function and this is achieved by minimizing $|\omega|^2$. Non-negative slack variables are introduced to account for training points that fall outside of the ε-insensitive zone. That is:

$$\begin{gathered} minimize\ \frac{1}{2}|\omega|^2 + C\sum_{i=1}^{N}(\xi_i + \xi_i{}^*) \\ s.t. \begin{cases} y_i - \langle \omega \cdot x_i \rangle - b \le \varepsilon + \xi_i{}^* \\ \langle \omega \cdot x_i \rangle + b - y_i \le \varepsilon + \xi_i \\ \xi_i{}^*, \xi_i \ge 0 \end{cases} \end{gathered} \tag{2.30}$$

where C is a positive constant, and ε is the insensitive zone, both are chosen by the user. C is also referred to as the regression parameter or penalty parameter. Cherkassky and Ma[28] propose C be chosen as

$$C = \max\left(|\mu_Y + 3\sigma_Y|, |\mu_Y - 3\sigma_Y|\right) \tag{2.31}$$

where μ_Y and σ_Y are the mean and standard deviation of the training point responses. Hsu et al.[30] suggest a cross-validation approach to find C.

The parameter ε determines the width of the ε-insensitive zone and affects the complexity/flatness of the model. The values of ε should be tuned to the input data, but a reasonable starting value is found using

$$\varepsilon = \frac{c}{100}|\tilde{y}_{max} - \tilde{y}_{min}| \tag{2.32}$$

with c = 1 where $|\tilde{y}_{max} - \tilde{y}_{min}|$ is the range of the responses at the training points. The value of c can be tuned for the function. Cherkassky and Ma[28] propose ε be chosen as

$$\varepsilon = 3\sigma\sqrt{\frac{\ln N}{N}} \tag{2.33}$$

where σ is the standard deviation of the noise associated with the training point response values and N is the number of training points. This assumes the noise is known or can be determined. Cherkassky and Ma[28] suggest the following to estimate the unknown variance of noise using a k-nearest neighbor technique

$$\sigma^2 = \frac{N^{1/5}k}{N^{1/5}-1} \cdot \frac{1}{N}\sum_{i=1}^{N}(y_i - \hat{y}_i)^2 \tag{2.34}$$

where k is in the range [2,6] and $\sum_{i=1}^{N}(y_i - \hat{y}_i)^2$ is the squared sum of the residuals.

The optimization problem in Eq. (2.30) written as a Lagrangian function is

$$L = \frac{1}{2}|\omega|^2 + C\sum_{i=1}^{N}(\xi_i + \xi_i^*) - \sum_{i=1}^{N}\alpha_i(\varepsilon + \xi_i - y_i + \langle\omega \cdot x_i\rangle + b)\ )$$
$$- \sum_{i=1}^{N}\alpha_i^*(\varepsilon + \xi_i^* + y_i - \langle\omega \cdot x_i\rangle - b) - \sum_{i=1}^{N}(\eta_i\,\xi_i + \eta_i^*\xi_i^* \tag{2.35}$$

where η_i and η_i^* are additional slack variables. From Lagrangian theory, necessary conditions for α to be a solution are listed below

$$\partial_b L = \sum_{i=1}^{N}(\alpha_i^* - \alpha_i) = 0 \tag{2.36}$$

$$\partial_\omega L = \omega - \sum_{i=1}^{N}(\alpha_i^* - \alpha_i)\,x_i = 0 \tag{2.37}$$

$$\partial_{\xi_i} L = C - \alpha_i - \eta_i = 0 \tag{2.38}$$

$$\partial_{\xi_i^*} L = C - \alpha_i^* - \eta_i^* = 0 \tag{2.39}$$

Substituting Eqs. (2.36) - (2.39) into Eq. (2.30) gives the dual form optimization problem

$$Maximize \begin{cases} -\frac{1}{2}\sum_{i,j=1}^{N}(\alpha_i - \alpha_i^*)(\alpha_j - \alpha_j^*)\langle x_i \cdot x_j\rangle \\ -\varepsilon\sum_{i=1}^{N}(\alpha_i + \alpha_i^*) + \sum_{i=1}^{N} y_i(\alpha_i - \alpha_i^*) \end{cases}$$
$$s.t. \begin{cases} \sum_{i=1}^{N}(\alpha_i - \alpha_i^*) = 0 \\ (\alpha_i - \alpha_i^*)\,\epsilon\,[0, C] \end{cases} \tag{2.40}$$

Eq. (2.37) is rewritten as

$$\omega = \sum_{i=1}^{N} (\alpha_i{}^* - \alpha_i)\, x_i \tag{2.41}$$

The linear regression first expressed in Eq. (2.29) is written as

$$f(x) = \sum_{i=1}^{N} (\alpha_i - \alpha_i{}^*)\, \langle x_i \cdot x_i \rangle + b \tag{2.42}$$

Clarke et. al[31] summarize the process of transforming the problem into dual form by stating:

> "*Transforming the optimization problem into dual form yields two advantages. First, the optimization problem is now a quadratic programming problem with linear constraints and a positive definite Hessian matrix, ensuring a unique global optimum. For such problems, highly efficient and thoroughly tested quadratic solvers exist. Second, as can be seen in Eq. [(2.40)], the input vectors only appear inside the dot product. The dot product of each pair of input vectors is a scalar and can be preprocessed and stored in the quadratic matrix* $M_{ij} = (\langle x_i x_j \rangle)_{ij}$. *In this way, the dimensionality of the input space is hidden from the remaining computations, providing means for addressing the curse of dimensionality*."

A nonlinear regression model can be developed by replacing the dot product $\langle \boldsymbol{x_i} \cdot \boldsymbol{x_i} \rangle$ with a kernel function, *k*, rewriting the optimization problem in Eq. (2.40) as

$$Maximize \begin{cases} -\frac{1}{2} \sum_{i,j=1}^{N} (\alpha_i - \alpha_i{}^*)(\alpha_j - \alpha_j{}^*)\, k(x_i, x_j) \\ -\varepsilon \sum_{i=1}^{N} (\alpha_i + \alpha_i{}^*) + \sum_{i=1}^{N} y_i (\alpha_i - \alpha_i{}^*) \end{cases} \quad s.t. \begin{cases} \sum_{i=1}^{N} (\alpha_i - \alpha_i{}^*) = 0 \\ (\alpha_i - \alpha_i{}^*)\, \epsilon\, [0, C] \end{cases} \tag{2.43}$$

Replacing the dot product with a kernel function in the approximation function Eq. (2.42) gives the nonlinear SVR approximation as

$$f(x) = \sum_{i=1}^{N} (\alpha_i - \alpha_i{}^*)\, k(x_i, x_j) + b \tag{2.44}$$

Common Kernel functions include the following:

- Linear: $k(x_i, x_j) = x_i{}^T, x_j$
- Polynomial: $k(x_i, x_j) = (\gamma\langle x_i \cdot x_j\rangle + r)^d \;\; \gamma > 0$
- Gaussian: $k(x_i, x_j) = \exp\left(-\frac{\|x_i - x_j\|^2}{2p^2}\right)$
- Radial Basis Function: $k(x_i, x_j) = \exp\left(-\gamma\|x_i - x_j\|^2\right) \qquad \gamma > 0$
- Sigmoid: $k(x_i, x_j) = \tanh\left(\gamma\langle x_i \cdot x_j\rangle + r\right)$

where γ,*d*, *p*, and *r* are kernel parameters and should be adjusted by the user for each data set. Listed below are some insights about setting kernel parameters:

1) The polynomial degree *d* is typically chosen to be 2. Gunn[29] uses *r* = 1 to "avoid problems with the hessian becoming zero".
2) Hsu et al.[30] use a cross-validation approach to determine γ for RBF. This procedure could be applied to γ for other kernels as well as other kernel parameters.
3) Cherkassky and Ma[28] suggest p for the Gaussian kernel (they call it RBF, the formulation is the same as "Gaussian" here) as $p \sim (0.1 - 0.5) * range(x)$ for single variable problems and $p^L \sim (0.1 - 0.5)$ for multi variable problems where *L* is the number of variables and all input variables are normalized to [0,1].

It should be noted that the "Gaussian" kernel here is sometimes referred to as "Radial Basis Function" and "Gaussian Radial Basis Function" in the literature. Experience shows that SVR metamodels are highly sensitive to tuning parameters. The suggestions expressed in this discussion may not result in an acceptable accuracy level.

The reader is encouraged to perform SVR tuning to ensure an accurate model for the selected response.

The SVR MATLAB toolbox developed by Gunn[29] was used in this study and the Linear kernel is used. The tuning parameters explored within SVR are penalty parameter, *C* and ε-insensitive zone parameter, *c*.

Optimized Ensemble (EN)

An ensemble of metamodels combines predictions from several stand alone metamodels such as the ones presented above. Ensemble metamodels are more accurate than the individual members but also more computationally expensive. The general form of an ensemble is a weighted sum of the predictions of separate metamodels. In mathematical form, this is expressed as

$$\tilde{f}(x) = \sum_{i=1}^{M} w_i(x)\, \hat{f}_i(x) \tag{2.45}$$

where $\tilde{f}(\boldsymbol{x})$ is the ensemble prediction, $\boldsymbol{x}$ is the vector of input variables, *M* is the number of metamodels used to build the ensemble, w_i is the weight factor for the *ith* metamodel, and $\hat{f}_i$ is the prediction of the *ith* metamodel. The weight factors must sum to one

$$\sum_{i=1}^{M} w_i(x) = 1 \tag{2.46}$$

Selection of the weight factors is the most important step when constructing an accurate ensemble. Acar and Rais-Rohani[22] developed an ensemble minimizing the error by finding the optimal weight factors. In mathematical form, this is expressed as

$$\begin{gathered} \min \tilde{\varepsilon} = Err\left\{\tilde{f}\left(w_i, \hat{f}_i(x^k)\right) f(x^k), k = 1 \in \mathrm{N}\right\} \\ s.t. \sum_{i=1}^{M} w_i = 1 \end{gathered} \tag{2.47}$$

where *Err{ }* is the error metric that finds error of the ensemble predictions, $\tilde{f}$, $f(x^k)$ is the actual response at the training point x^k, and *N* is the number of training points. In this study the prediction error was based on the Generalized Mean Square Error (GMSE) metric defined as

$$GMSE \equiv \frac{1}{N}\sum_{i=1}^{N}\left(fi - \hat{f}_i\right)^2 \tag{2.48}$$

where *N* is the number of design points, fi is the actual response, and $\hat{f}_i$ is the predicted response from each metamodel.

CHAPTER III

CRASH SIMULATIONS

A full-scale 1996 Dodge Neon, FE model (v07 in LS-DYNA) is used as the vehicle model. This model was developed at the National Crash Analysis Center (NCAC) and is a public domain model downloadable from the NCAC website[32]. This model, seen in Figure 3.1, contains no interior panels or seats and was designed for crash analysis. The glass windows and windshields are modeled but not designed to break or crack.

Rubbers, foams, and metals are all used to define the 336 separate parts in the model. Most structural components are Belytchko-Tsai reduced integration shell elements made of steel defined using Mat 24 in LS-DYNA [33]. The vehicle is made up of 270,768 elements of which 267,786 are shells, 2,852 are solids, and 122 are beams. It has approximately 1.7 million degrees of freedom. Concentrated mass elements are positioned throughout the model to approximate the mass distribution of the actual

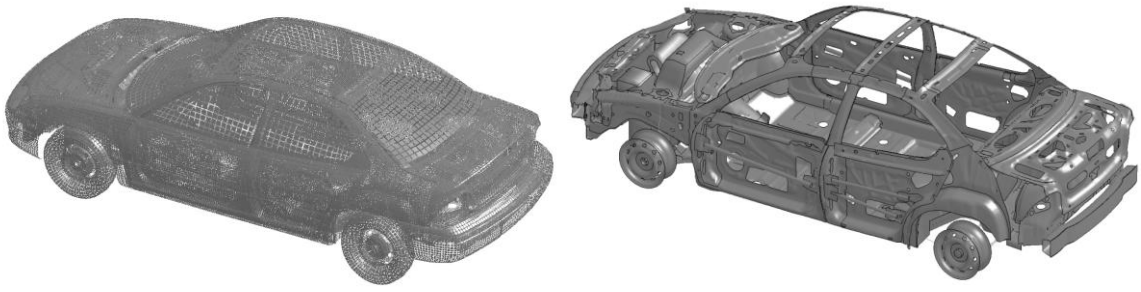

(a) (b)

Figure 3.1 Dodge Neon FE Model with (a) Exterior Panels and Mesh (b) Exterior Panels and Tires Removed

vehicle giving a total vehicle mass of 1,333 kg. These mass elements also account for other components of the vehicle such as interior panels, instrumentation, seats, and dummies that would be included in a real crash setup.

The model uses the spot-weld constraint in LS-DYNA for the majority of the connections between parts and uses both rigid and non-rigid constraints to connect other parts. Modal analysis is difficult to perform with this model because of the number of parts and type of connections. Each part has a unique material identification number although the material may be the same as in other parts. This makes it easy to identify parts and extract results using the material.

A gravitational load is applied to all parts in the model. This model was validated by NCAC for FFI crash scenarios [34]. Responses such as acceleration, velocity, and wall force were compared with test results to validate the model.

Impact Scenarios

This model was incorporated into simulations for Side impact (SIDE) and 40% Offset Frontal Impact (OFI) scenarios in addition to FFI providing three impact cases. These models followed the FMVSS for impact location, angle, and the vehicle/barrier used. The FFI scenario has an impact speed of 56 km/hr (35 mph) into a rigid barrier with the bumper impacting squarely with the barrier. This simulates a directly head-on collision with a vehicle traveling at the same speed or impact into a rigid or nearly rigid structure. The SIDE scenarios simulate the vehicles response when impacted by another vehicle when one ignores a stop sign or traffic light. Speed for validation and testing for SIDE was 52 km/hr (32 mph). FMVSS specify a 27° impact angle relative to the length of the car that is hit by deformable trolley with a crushable honeycomb material

simulating the front of another vehicle for SIDE. The OFI simulations were validated at 60 km/hr (37 mph) based on available test data and used for the model without dummy at

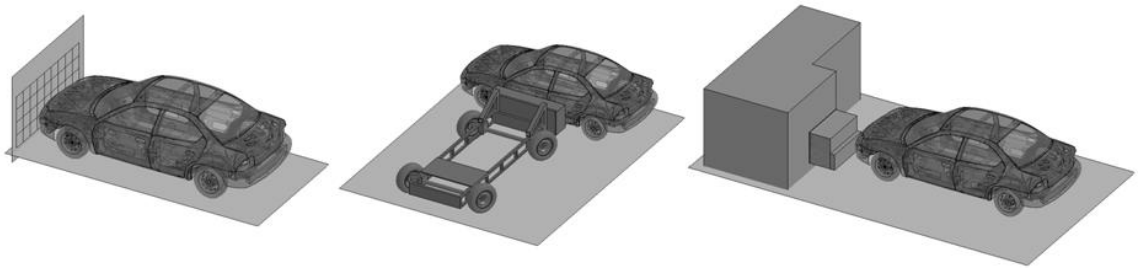

(a) (b) (c)

Figure 3.2 Crash Scenarios (a) FFI, (b) SIDE, and (c) OFI

56 km/hr (35 mph) to coincide with FFI simulations. The Neon model impacts a deformable honeycomb material barrier in front of a rigid wall with 40% of the vehicle-front impacting the barrier. This simulates impacting another vehicle at an offset rather than directly head on. Figure 3.2 shows the Neon model in each crash simulation.

A simulation of each scenario was performed in LS-DYNA to validate the models. Acceleration curves at the left rear sill for OFI and at the middle of the B-pillar

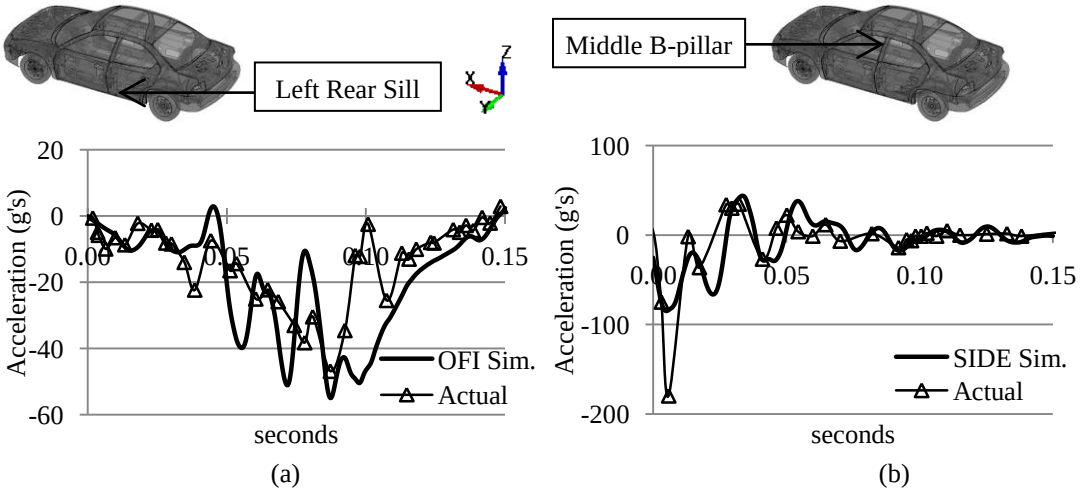

Figure 3.3 Validation of (a) OFI X-Acceleration at Left Rear Sill (b) SIDE Y-Acceleration at Middle B-Pillar

for SIDE are shown and compared to physical test results [35, 36] in Figure 3.3. The SIDE test results are from a passenger side impact (with the dummy in the passenger seat) while this model uses a driver side impact. Validation of the FFI model beyond what was done by NCAC was not performed for this model. Test results for the FFI scenario can be found in Ref. 37. This figure shows that the general shapes of the curves are the same but peak values differ as a result of filtering and the method used to capture the data. A 9th order low-pass Butterworth filter at 60 Hz was used to extract the data. This filter was chosen to give a smooth curve that produced similar results to the SAE J211 class filters used in the test results. The Butterworth filter is also available for use in MATLAB. The test result data was taken from a pdf image of the test report using a point-select software where peaks, valleys, and the general shape of the curves were captured. The locations of these observation points were determined by the position of accelerometers in the actual testing. Appendix A contains a portion of the FFI LS-DYNA keyword input cards.

Design Variables

Twenty-two parts, as shown in Figure 3.4, are chosen as the design parts were primarily chosen based on significant contributions to energy absorption, see Figure 3.5.

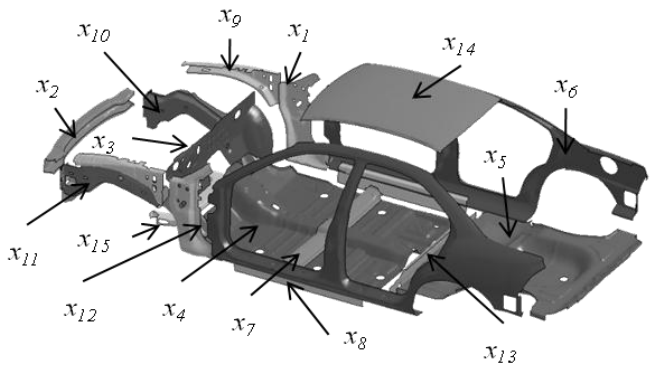

Figure 3.4 Selected Vehicle Parts and Associated Design Variables

and structural stiffness. Parts such as the Rear Plate (*x13*) and Roof (*x14*) were selected for their contributions based on findings in Leiva et al.[38] The internal energy absorption of each part is calculated from simulation results using each of the three impact scenarios. Selected parts account for approximately 40% of the total vehicle energy absorption in all three scenarios and have a mass of 105 kg compared to 1,333 kg for the vehicle, about 8%.

Shell element thicknesses of these parts, as noted in Table 3.1, are used as design variables with thicknesses of the parts in the NCAC model serving as the baseline values. Limits on thickness were set to 50% above and below the baseline thickness for each part. This was done to maintain realism through manufacturability. A total of fifteen design variables result from the twenty-two parts because of symmetry in the vehicle.

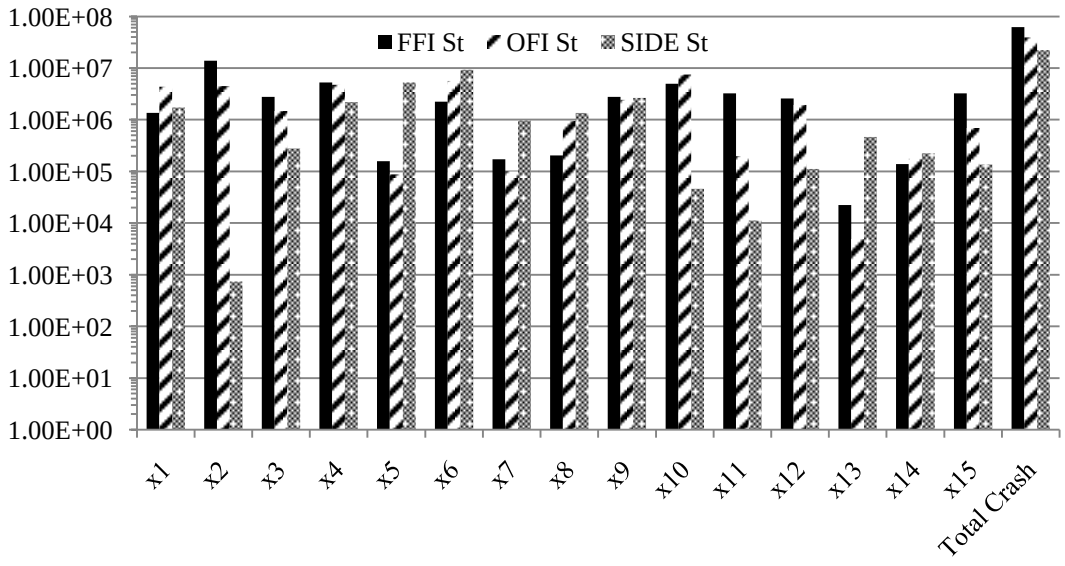

Figure 3.5 Part Internal Energy Contribution and Total Crash Internal Energy

Crash Test Dummy Incorporation

A crash test dummy model was included in the Neon model described previously. This provides the ability to obtain responses closely linked to occupant injury during crash events. The LS-DYNA dummy models used are distributed by Livermore Software Technology Corporation (LSTC), the creators of LS-DYNA. These models are available to anyone with an active LS-DYNA license from the LSTC models website [39].

Interior components were put into the Neon model to capture the dummies interactions with them. The interior included non-structural panels on the door and dashboard, the steering wheel assembly and mounting structure, and a non-rigid seat with seatbelt. Only the front interior on the driver side of the vehicle was included. Concentrated mass elements were removed from the NCAC v07 Neon model to allow for the added mass of the dummy and interior. Mass elements were taken from the front, driver's side of the vehicle to maintain the mass distribution. The FFI and OFI models have a total mass with the interior and dummy of 1,317 kg and the SIDE model has a mass of 1,310 kg because there is a difference in the mass of the dummy models used in frontal and side impacts.

There are no airbags installed in this model and the seatbelt is 303 of the 1-dimensional LS-DYNA seatbelt elements with one degree of freedom along the length. A retractor is incorporated to remove slack from the belt before impact and locks at 0.02 seconds but a pretensioner is not included. This seatbelt model provides adequate realism without being as complex as using a design with 2-dimensional shell elements to model the seatbelt.

A 50th percentile male Hybrid III (H3) dummy model was used for FFI and OFI simulations while a 50th percentile male US Side Impact Dummy (USSID) was used in SIDE simulations. Both of these dummies were validated by the distributor using benchmark tests on actual crash test dummies. Each dummy is positioned in the vehicle's driver seat following locations specified in the test reports. Contact is defined between the legs and back to the seat for frontal and side impacts. Contact is also defined for knees to the underside of the dashboard and feet to the floorboard for frontal impacts and door to the dummy's torso for side impacts. Figure 3.6 shows the added interior with the dummy models positioned.

Validation simulations were run for each of the impact scenarios. Simulation results were then compared to the results in the test reports and to the model without the interior and dummy. Steering wheel airbags were present in the FFI and OFI test results but no airbags were present in the SIDE test results. A comparison of the resultant acceleration of the dummy head to test results and at a location on the middle of the B-pillar to the model without the dummy for FFI can be seen in Figure 3.7.

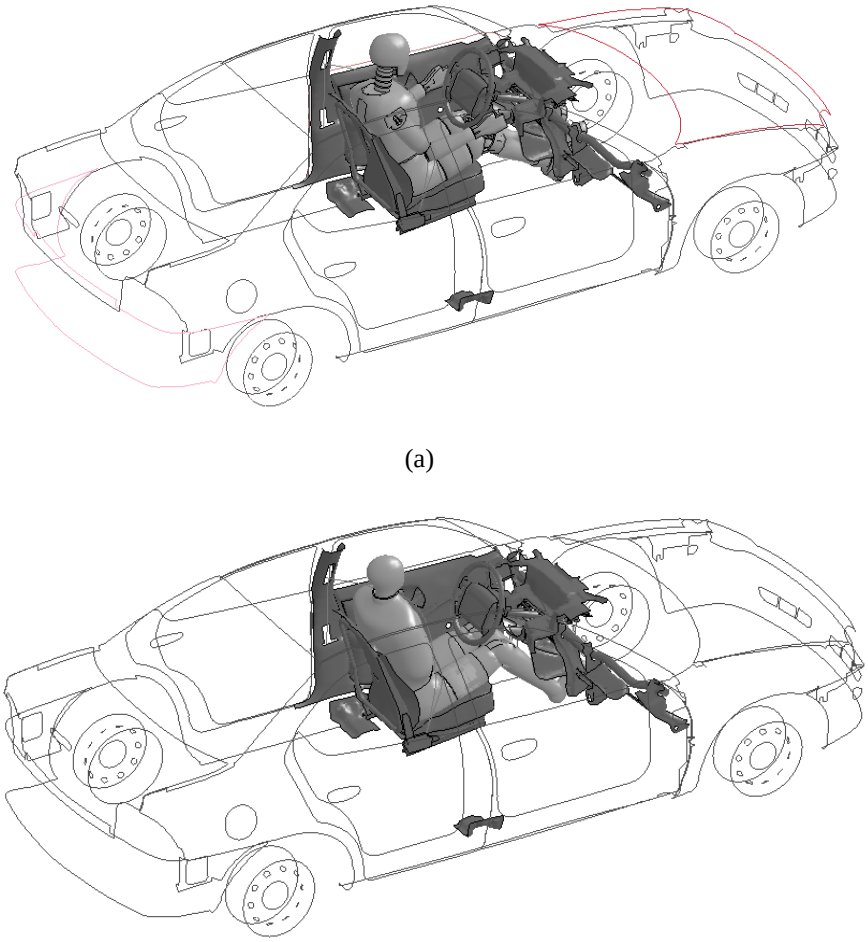

(a)

(b)

Figure 3.6 Added Interior Parts with Positioned Dummies (a) H3 for FFI and (b) USSID for SIDE

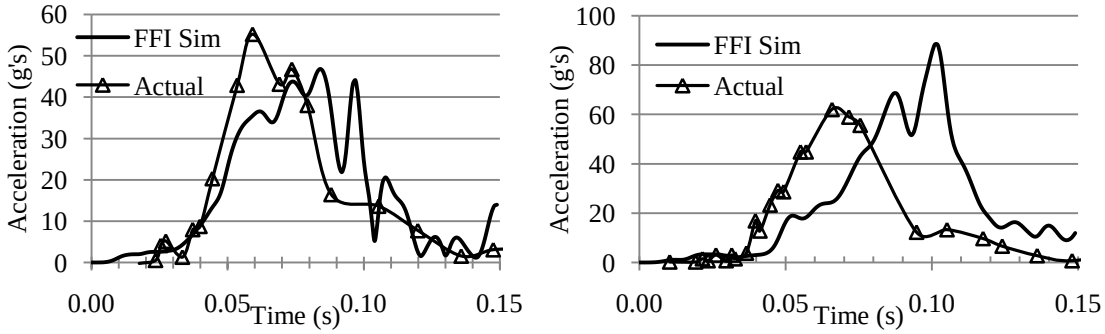

(a) (b)

Figure 3.7 FFI Dummy Model's (a) Chest Resultant Acceleration and (b) Dummy Head Resultant Acceleration Compared to Test Results

Figure3.7(a) shows similar peak values and overall shape between the two curves for resultant chest acceleration while Figure 3.7(b) shows that peak resultant acceleration of the simulation is shifted to the right compared to the test results. The simulation's second peaks seen around 0.1 seconds in this figure are likely the result of the chest hitting the steering wheel between 0.08 and 0.09 sec. The chest deflection time-history curve, seen in Figure 3.8, appears to be leveling off at a deflection around 40 to 42 mm before suddenly increasing to 56 mm. The maximum chest deflection measured in the actual test was 40 mm. This suggests a problem in the modeling of the seat and/or seatbelt for frontal impact simulations since a primary function of the seatbelt is to prevent the dummy from hitting the steering wheel.

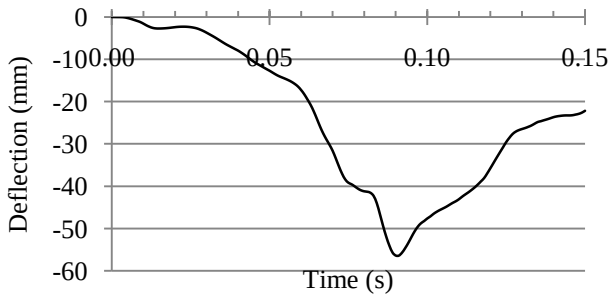

Figure 3.8 FFI Simulation Chest Deflection Curve

Acceleration curves for SIDE are compared in Figure 3.9. Figure 3.9(a) shows that the dummy pelvis y-acceleration curve is nearly identical for the model and test results. Figure 3.8(b) shows the resultant acceleration comparison of the dummy ribs. The lower rib (Lwr Rib) corresponds to the accelerometer location in the test setup where both upper and lower rib accelerations were measured while only one rib acceleration was measured in the simulations. The peak values are nearly identical but with a time shift of a difference in data-recording initialization.

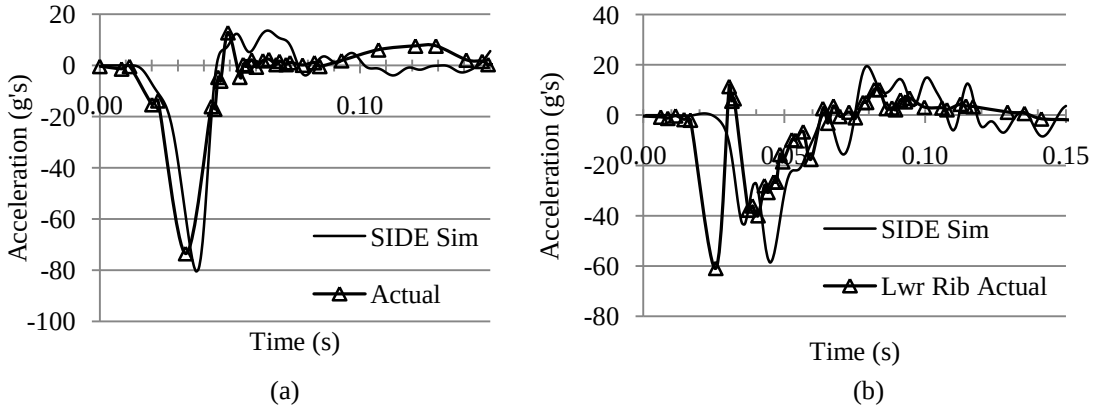

Figure 3.9 SIDE Dummy Model's (a) Pelvis Y-Acceleration and (b) Rib Y-Acceleration Compared to Test Results

Figure 3.10(a) shows the resultant acceleration at the middle of the B-pillar location for the model with and without the dummy for OFI. The dummy model response shows a similar curve shape to the model without the dummy but significantly larger peak values. This can be partially attributed to a larger speed velocity, 60.3 km/hr for the dummy model compared to 56 km/hr for the model with no dummy. Figure 3.10 (b) shows that the model with the dummy has a larger peak velocity occurring later in the

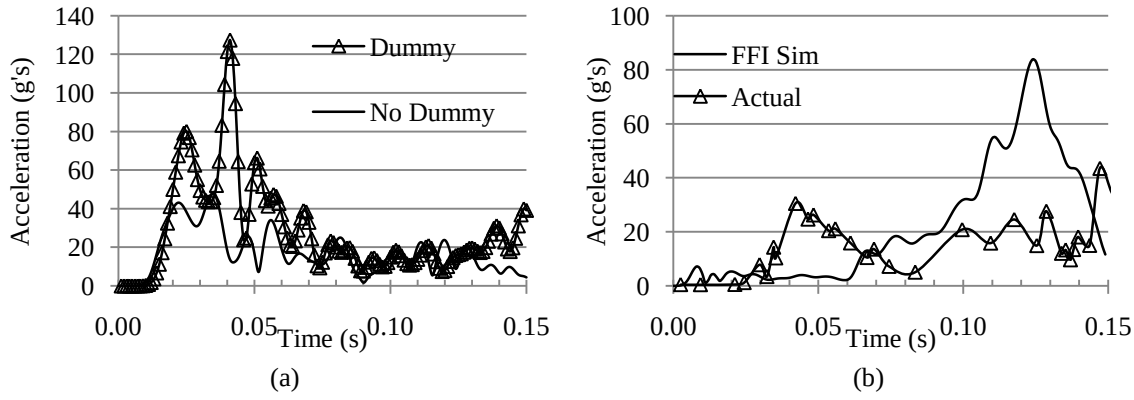

Figure 3.10 OFI Occupant Model Comparison of (a) Resultant Acceleration at the Middle of the B-Pillar to the Model Without Dummy and (b) Dummy Head Resultant Acceleration to Test Results

simulation. These results also suggest a problem with this model for frontal impacts. Only a limited set of dummy responses discussed in the next section were used in the design optimization study given the discrepancies found between the FFI and OFI responses of the model with a dummy and the test results.

Design Responses

Vehicle-based responses are intrusion distances at the toeboard and dashboard for FFI and OFI and at the door for SIDE (Int Toe, Int Dash, and Int Door), resultant acceleration at a location on the B-pillar in all three scenarios (Accel), and internal energy absorption of the selected parts in all three scenarios (Int Eng). Locations of these responses can be seen in Figure 3.11. These responses were chosen because of their relevance to occupant safety. Intrusion into the cabin can cause injuries such as to the legs in frontal impacts. The acceleration response location was chosen to be near an approximate head location of the driver during a crash.

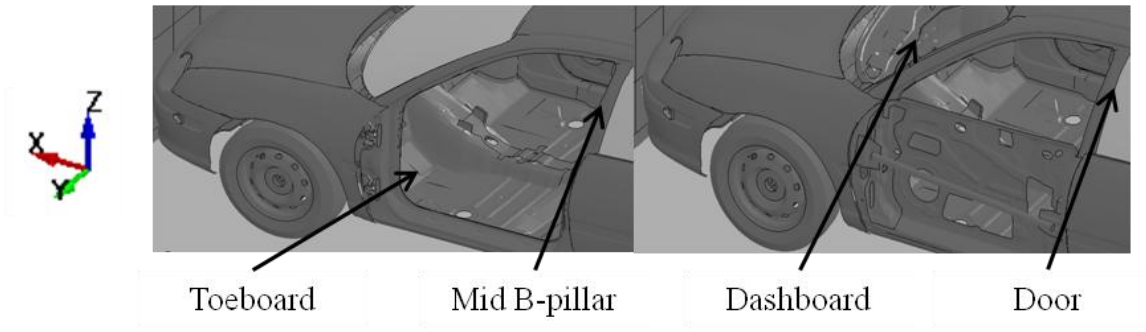

Figure 3.11 Selected Vehicle Response Locations

Intrusion distance was calculated by measuring the distance between twenty nodes at each response location and a reference node on the opposite side of the car before and after the crash and then finding the difference. An average over the twenty

nodes was used as the intrusion distance response. A 9th order low-pass Butterworth filter at 60 Hz was applied to the acceleration curves for twenty nodes at the selected location, the resultant found, an average over the twenty nodes taken, and the maximum value found to represent an acceleration response. The internal energy response is the sum of the internal energy at the end of the simulation for the selected parts.

Dummy-based responses are based on FMVSS specified upper limits on a number of injury criteria for both frontal and side impacts. The limits are set based on test results to determine human responses to conditions in a crash environment. Frontal injury criteria used as responses are Head Injury Criteria (HIC), maximum upper leg axial force (Femur Force), maximum neck axial force (Neck Force), and peak chest deflection (Chest Def). Side impact injury criteria used are Thoracic Trauma Index (TTI), maximum pelvic acceleration (Pelvis Accel), and peak rib deflection (Rib Def).

The HIC was developed to measure the likelihood of an injury to the head. An HIC limit is specified as a requirement in the FMVSS for both frontal and side impact scenarios. It is only used as a response for frontal impacts here because the USSID used is not calibrated for head and neck measurements. HIC is expressed as

$$HIC36 = max\left[\frac{1}{t_2-t_1}\int_{t_1}^{t_2} a dt\right]^{2.5}(t_2 - t_1) \tag{3.1}$$

where t is time and a is the resultant acceleration of the head with $(t_2 - t_1) = 36\, ms$. A time window size of 15 ms can be used as well but 36 ms is used in this study. The larger the HIC value, the more likely a serious injury will occur. Resultant head acceleration is calculated from differentiating the velocity versus time curve of the FE model part representing the skull. This method was done because of difficulty extracting nodal

accelerations and velocities of the accelerometer positioned in the middle of the head. A 9th order low-pass Butterworth filter at 120 Hz was used to filter the data.

The neck force and femur force were measured at the joints connecting the neck to skull and leg to pelvis, respectively. The positive axial directions are away from the head for the neck force and towards the feet for the femur force. A maximum value was taken from the filtered acceleration data using the same type filter as for the head acceleration. Femur force was recorded for both legs with the maximum force between them used as the response value. Chest deflection was determined by measuring the change in length of a spring running from sternum to spine in the FE model. Figure 3.12(b) shows the H3 dummy model with the parts used for accelerations darkened.

Thoracic Trauma Index (TTI) is specified in the FMVSS for side impact scenarios. It is defined as

$$TTI = 0.5(Rib_{ay} + Spine_{ay}) \tag{3.2}$$

where Rib_{ay} is the y-acceleration (y-axis is from shoulder to shoulder in a forward facing dummy) at of the ribs closest to the door where impact occurs and $Spine_{ay}$ is the y-acceleration at of the ribs closet to the door where impact occurs. Filtered data using a 9th order low-pass Butterworth filter at 120 Hz was used from the differentiation of the part y-velocity. The same procedure was used to find the maximum, resultant, pelvis acceleration. Rib deflection was determined from the change in length of a spring stretching between the ribs in the y-direction. Figure 3.12(a) shows the USSID model with the parts used for acceleration darkened.

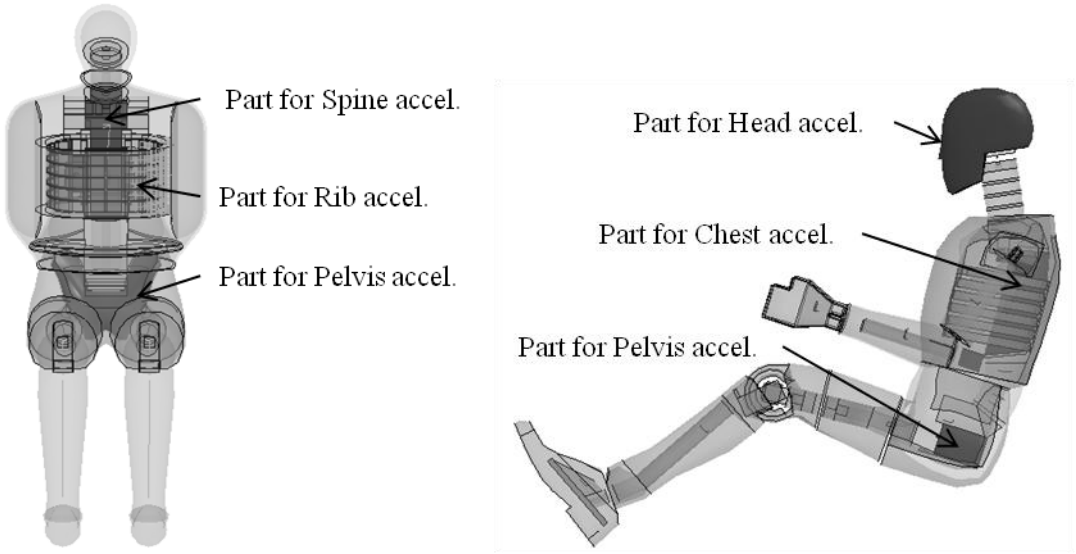

(a) (b)

Figure 3.12 Dummy Models with Shaded Acceleration Locations (a) USSID for SIDE (b) H3 for OFI and FFI

Material Substitution

AZ 31 magnesium alloy was selected to replace the baseline steel sheet formed parts in the Neon model. Mat 124 in LS-DYNA[33] was used to model it based on work by Wagner et al.[40]. This material model allows the definition of separate stress-strain curves for compression and tension. These stress-strain curves were taken from quasi-static experimental data at 22°C. AZ31(*TD*) was used for the tension curve where *TD* is *transverse direction.*This data was unavailable for AZ 31 under compressive loading so a relation of the ratio of AM 30 under compression and tension along with AZ 31 was used to approximate a curve for AZ 31 compression as

$$AZ31(RD)_{comp} = \frac{AZ31(RD)_{ten}}{AM30\ (ED)_{ten}} * AM30(ED)_{comp} \tag{3.3}$$

where *RD* is rolled direction, *ED* is extruded direction, *ten* is tension, and *comp* is compression. Figure 3.13 shows the stress-strain curves for AM 30 and AZ 31.

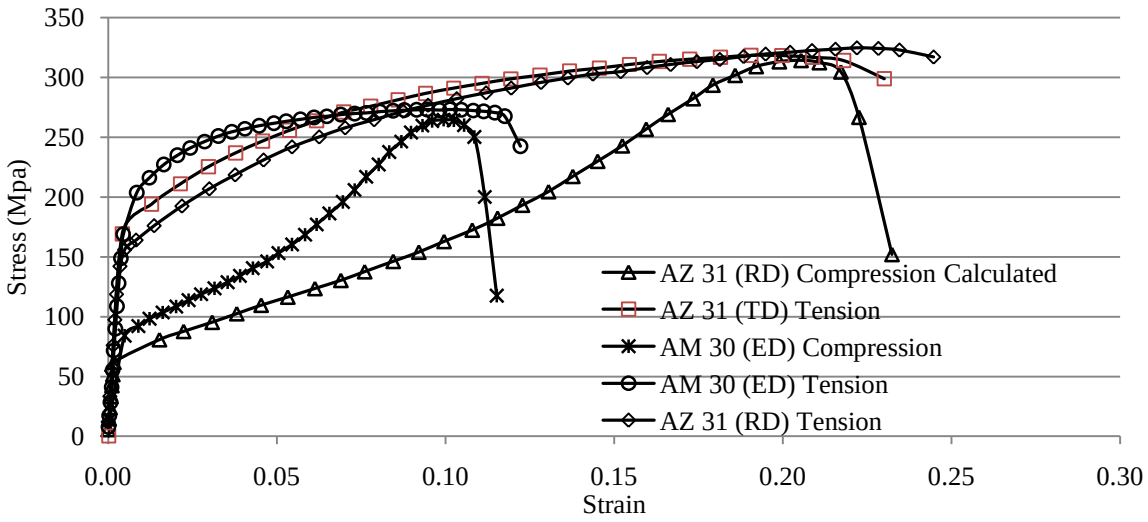

Figure 3.13 Magnesium Quasi-Static Stress-Strain Curves at 22°C

Material substitution was performed by changing the material of the twenty-two design parts from steel to magnesium and leaving the other parts in their base material. Seven different steel materials are used to define the 22 selected parts in the Neon FE model but only one magnesium model is used for each of the selected parts. The thicknesses of these magnesium replacement parts were selected to maintain the total internal energy absorption of the steel baseline parts in the model without the dummy and interior. This was done by using the relation of toughness and thickness shown in Eq. 3.4 for each selected part. An average of the thicknesses found using the toughness under compression and the toughness under tension was used. Magnesium thicknesses were found from

$$t_{Mg} = t_{St} \frac{T_{St}}{T_{Mg}} \tag{3.4}$$

where t_{Mg} and t_{St} are the thicknesses of magnesium and steel respectively, and T_{Mg} and T_{St} are the toughness values of steel and magnesium. Toughness was calculated from

integrating the stress-strain curves for each material from 0 to 0.3 strain. Thicknesses of the selected parts are found in Table 3.1 for the steel and magnesium designs.

Table 3.1 Part Thicknesses (in mm) for Baseline Designs

Part	Design Variable	St Base	Mg Base
A-Pillar	x_1	1.611	2.597
Front Bump	x_2	1.956	5.975
Firewall	x_3	0.735	1.072
Front Floor Panel	x_4	0.705	1.136
Rear Cabin Floor	x_5	0.706	1.138
Outer Cabin	x_6	0.829	1.366
Cabin Seat Reinf.	x_7	0.682	1.099
Cabin Mid Rail	x_8	1.050	1.692
Shotgun	x_9	1.524	3.620
Inner Side Rail	x_{10}	1.895	3.966
Outer Side Rail	x_{11}	1.522	3.186
Side Rail Exten.	x_{12}	1.895	3.966
Rear plate	x_{13}	0.710	1.144
Roof	x_{14}	0.702	1.157
Susp. Frame	x_{15}	2.606	5.342

This material model also allows the definition of plastic strain to failure. Magnesium's behavior under compressive loads requires this parameter in order to provide a more accurate material response. A plastic strain to failure of 38% is used in this study following Wagner et al.[40]. A value of 19% was also considered. Table 3.2 compares the total internal energy absorption of the 22 selected parts for each crash scenario using 19% and 38% plastic strain to failure. This table shows that magnesium with 38% plastic strain to failure has total internal energy absorption closer to the steel baseline than the 19%. Strain rate effects were found to have a negligible effect on selected responses and part energy absorption and were not included. The material defined in this manner is not an exact magnesium material model but a surrogate.

Table 3.2 Total Internal Energy of Selected Mg Parts

Crash Scenario	St	Mg 19%	Mg 38%
FFI	6.23E+07	6.03E+07	6.36E+07
OFI	3.94E+07	3.69E+07	3.94E+07
SIDE	2.24E+07	1.94E+07	2.09E+07

Simulations of each crash scenario using the magnesium material model defined previously were performed. Figure 3.14 shows that the acceleration curves at the B-pillar response location for each scenario generally match in shape and peak values. Table 3.3 shows an overview of the responses for baseline simulations with both materials. The magnesium parts have significantly less mass than the steel parts and generally maintain or improve the internal energy absorption of the replaced parts but the intrusion distances

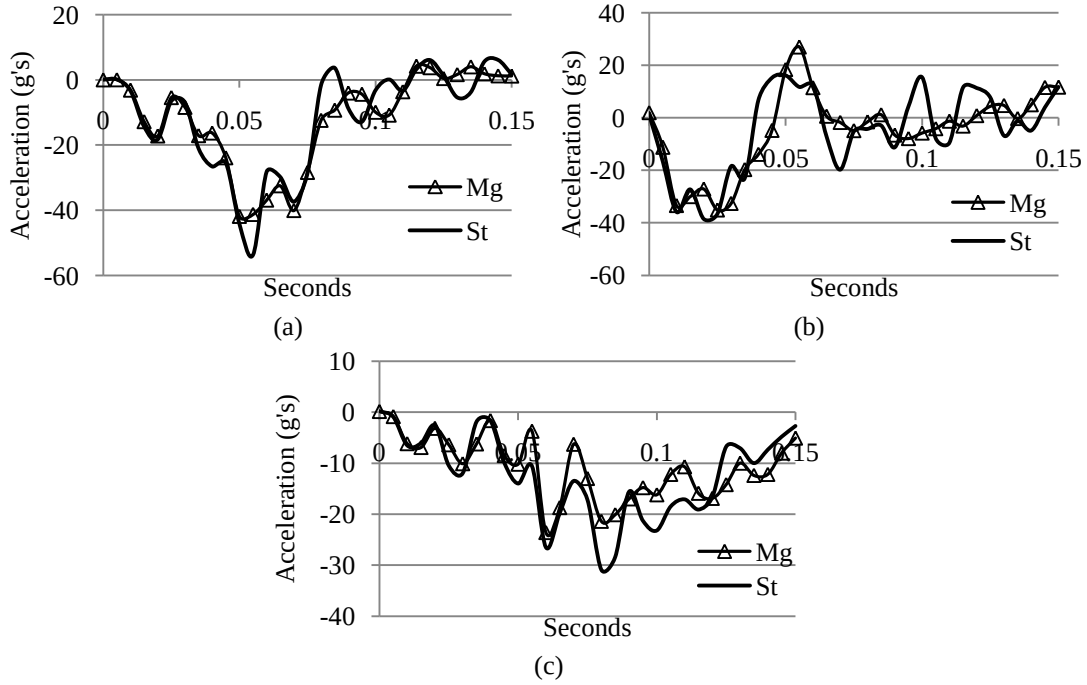

Figure 3.14 Acceleration at B-pillar Response Location-No Dummy (a) x-dir. FFI, (b), y-dir. SIDE, and (c) x-dir. OFI for Mg and St

are significantly larger than the steel parts. These responses and designs are treated as the baseline for comparison of the optimum designs when the model without dummy is used.

Table 3.3 Response Comparison for Baseline St and Mg

		St Base	Mg Base	% from St Base
FFI	Int Toe (mm)	157	295	87.9%
	Int Dash (mm)	122	186	52.3%
	Accel (g's)	63.5	49.2	-22.5%
	Int Eng (kJ)	62.3	62.3	0.1%
SIDE	Int Door (mm)	314	420	33.7%
	Accel (g's)	47.9	40.8	-14.9%
	Int Eng (kJ)	22.4	21.4	-4.3%
OFI	Int Toe (mm)	273	349	27.7%
	Int Dash (mm)	247	386	56.2%
	Accel (g's)	35.0	36.2	3.3%
	Int Eng (kJ)	39.4	39.2	-0.4%
	Mass (kg)	105.2	42.7	-59.4%

Magnesium defined in this manner was also applied to the models with the dummy and interior included. Simulations were run for each scenario to compare the steel dummy model with the magnesium dummy model. Acceleration results at the dummy head and B-pillar location for the FFI case can be seen in Figure 3.15. The B-pillar x-acceleration curves are similar for the first half of the simulation but differ in the last portion. The Mg head acceleration curve has a lower peak value than the St curve but have a similar shape. Figure 3.16 shows that for SIDE the y-acceleration curves at the B-pillar have a similar shape for St and Mg and the Dummy y-accelerations at the Rib location are nearly identical. OFI accelerations in Figure 3.17(a) show that x-acceleration at the B-pillar does not match and (b) shows the shape is similar but peak values are different.

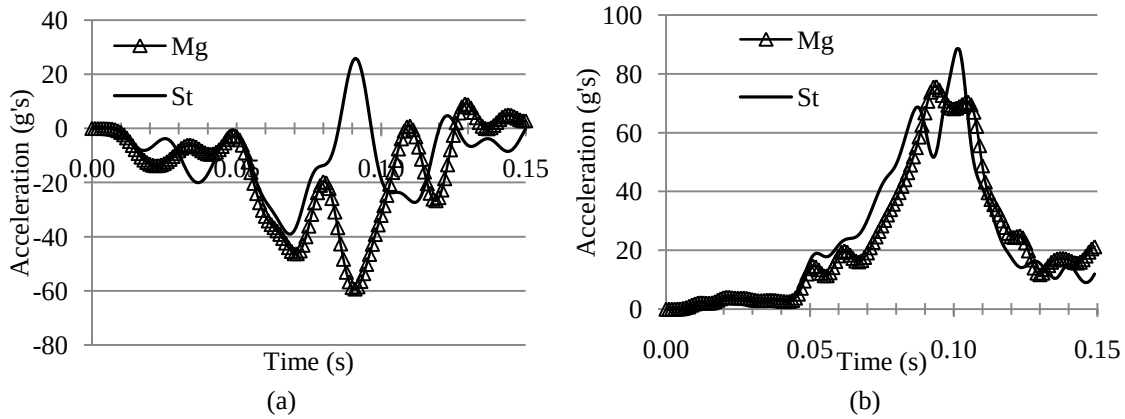

Figure 3.15 FFI Occupant Model Comparison of (a) x-Acceleration at the Middle of the B-pillar and (b) Dummy Head Resultant Acceleration for Mg and St

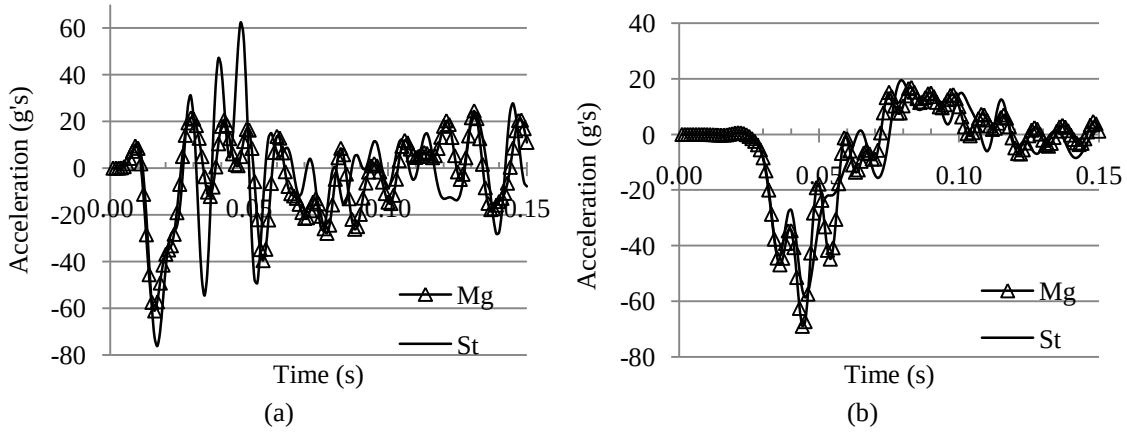

Figure 3.16 SIDE Occupant Model Comparison of (a) y-Acceleration at the Middle of the B-Pillar and (b) Dummy Rib y-Acceleration for Mg and St

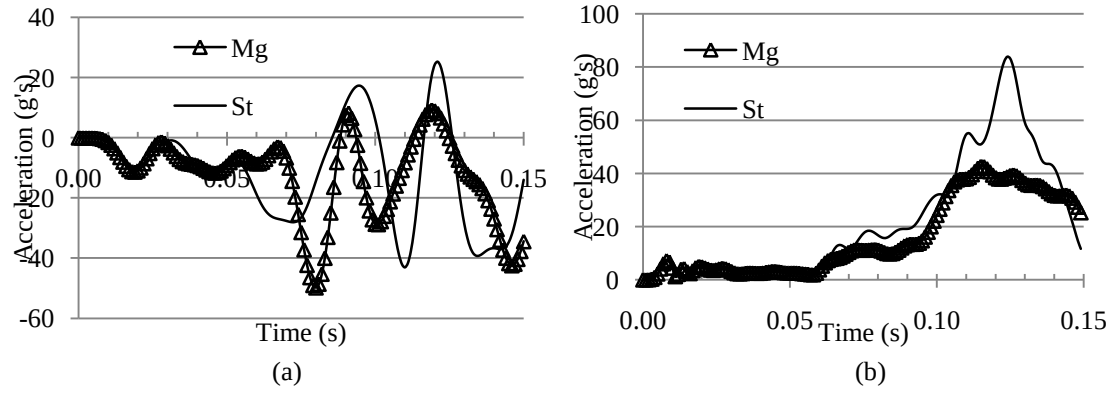

Figure 3.17 OFI Occupant Model Comparison of (a) x-Acceleration at the Middle of the B-pillar and (b) Dummy Head Resultant Acceleration

Dummy-based responses for the St and Mg baseline design along with test result values (for Steel) and FMVSS limits can be seen in Table 3.4. All FFI responses are larger than the test results and generally below the FMVSS limit. OFI responses are generally above the test result values and below the FMVSS limit except neck force. OFI responses are all lower than their FFI counterparts. SIDE responses are fairly close to the test results and close to or below the FMVSS limit.

Table 3.4 Dummy Responses for Mg and St, Test Results for St, and FMVSS Limits

			Test Results (St)	Simulation (St)	FMVSS Limit	Simulation (Mg)
Frontal	HIC36	FFI	610	1167	1000	949.4
		OFI	111.5	891.6		891.6
	Femur Force	FFI	6859 N	8646 N	10008 N (2250 lb)	6600 N
		OFI	4273.5 N	5406.3 N		5406N
	Neck Force (compression)	FFI	2000 N	5260 N	4000 N	4054 N
		OFI	1532.7 N	4498.7 N		4500 N
	Chest Deflection	FFI	40 mm	56.4 mm	63 mm	35.9 mm
		OFI	N/A	15 mm		15 mm
Side	Rib Deflection		N/A	42.3 mm	44 mm	44.9 mm
	Pelvis Acceleration		73 g's	82.7 g's	130 g's	77.8 g's
	TTI		65 g's	60.8 g's	85 g's	65.8 g's

Dummy responses for the FFI and OFI models again show discrepancies between simulation results and test results. These differences are likely the result of the chest to steering wheel contact as discussed in a previous section caused by inadequacies in the seatbelt model and possibly the seat. The three SIDE responses shown in Table 3.4 are used as design responses in Chapter V but no frontal dummy responses are used.

CHAPTER IV

OPTIMIZATION WITHOUT DUMMY MODEL

The overall objective of this optimization process is to find a design that minimizes vehicle weight through the selected parts but maintains the crashworthiness of the baseline steel model without the dummy and interior. Vehicle-based responses are discussed first followed by discussion of the metamodel tuning results and the optimization problems.

The eleven vehicle-based responses presented in Chapter III and total mass of the selected parts provide objectives and constraints for design optimization. Mass is determined by dividing the initial mass of the baseline part by its initial thickness. This coefficient is multiplied by a new thickness for that part to determine the part's new mass. A metamodel is not used for calculating mass while a metamodel is used to calculate each nonlinear response.

Latin Hypercube Sampling was used to create a DOE table with forty-five points. The baseline design point was added for a total of forty six design points. Limits on the design variables were 50% above and below the baseline. DOE simulations were performed for all three impact types and both materials for a total of 276 simulations for this chapter.

Metamodel Tuning Parameters

The metamodel techniques discussed in Chapter II were built and tuned for each of the eleven responses and then used to create an optimized ensemble. The first step of this process was determining the most accurate combination of tuning parameters for each response and material. This was done by defining a list of possibilites for each tuning parameter. A metamodel was then built and tested for accuracy using all combinations of the tuning parameters.

Cross-validation GMSE was used to measure the error of each model. A cross-validation technique is used when the number of points and their function evaluations is limited through availability or by cost of obtaining them, such as for full-scale crash simulations. Cross-validation builds a metamodel using all except one of the available training points and then measures the error of the prediction at the point that was left out. This is repeated with each point being left out and then the error is averaged to provide the error of that metamodel. GMSE is defined as (same as Eq. (2.48))

$$GMSE \equiv \frac{1}{N}\sum_{i=1}^{N}\left(fi - \widehat{f_i}\right)^2 \tag{4.1}$$

where N is the number of design points, fi is the actual response, and $\widehat{f_i}$ is the predicted response from each metamodel.

The tuning parameters tested for PRS were a first, second, and third degree polynomial. There are no tuning parameters for GP explored here. RBF tuning parameters are the basis function (i.e., *Thin Plate*, *Gaussian*, *Multiquadric*, and *Inverse Multiquadric)* and parameter *c*. Each of the four basis functions were explored with $c \in \{0.05, 0.1, 0.15, \ldots, 1\}$. The tuning parameters of KR explored are the polynomial degree, regression function, the upper bound on θ (called c) , and the lower bound on

(called *b).* Zero and first degree polynomials were explored with $c \in \{0.011, 0.1, 1, 20\}$ and $b \in \{0.001, 0.1\}$. The regression functions considered were *cubic*, *exponential*, *gaussian*, *linear*, *spherical*, and *spline.* SVR tuning parameters explored were the penalty parameter (C) and ε-insensitive zone parameter (c) with $C \in \{0.1, 2, 5, 10\}$ and $c \in \{0.01, 1, 10, 100\}$.

An Optimized Ensemble was created using the tuned base metamodels by minimizing the GMSE of the ensemble. The weight factors of the optimized ensemble are shown in Table 4.1. KR and SVR are the metamodels that have the highest percentage contribution to the ensemble across all responses and both materials. KR is the only metamodel in the ensemble for intrusion at the dashboard for FFI and acceleration at the B-pillar for SIDE. Table 4.2 and 4.3 show the tuned metamodel parameters for steel and magnesium, respectively. See Appendix B for a portion of the MATLAB code written to tune the metamodels in this manner including the PRS and RBF metamodels.

Table 4.1 Optimized Ensemble Weight Factors

		FFI				SIDE			OFI			
		Int Toe	Int Dash	Accel	Int Eng	Int Door	Accel	Int Eng	Int Toe	Int Dash	Accel	Int Eng
St	PRS	0	0	0	0	0	0	0	0	0.56	0	0
St	GP	0.57	0.17	0	0.33	0.48	0	0	0.51	0	0	0
St	RBF	0.30	0	0	0	0.01	0	0	0	0	0.16	0
St	KR	0.13	0.59	0.41	0.54	0.11	0.57	0.59	0.14	0.44	0.54	0.58
St	SVR	0	0.24	0.59	0.13	0.40	0.43	0.41	0.35	0	0.30	0.42
Mg	PRS	0	0	0	0	0	0	0	0.01	0	0	0
Mg	GP	0	0	0	0	0.34	0	0.14	0	0.07	0.27	0.15
Mg	RBF	0.33	0	0	0.09	0.08	0	0	0	0	0	0
Mg	KR	0.67	1.00	0.30	0.36	0.55	1.00	0.86	0.57	0.56	0.10	0.31
Mg	SVR	0	0	0.70	0.55	0.03	0	0	0.42	0.37	0.63	0.55

Table 4.2 Tuned Metamodel Parameters for St

Steel		FFI				SIDE			OFI			
		Int Toe	Int Dash	Accel	Int Eng	Int Door	Accel	Int Eng	Int Toe	Int Dash	Accel	Int Eng
PRS	Poly. Degree	1	1	1	1	1	1	1	1	1	1	1
RBF	Parameter, *c*	1	1	0.2	1	1	0.05	0.05	1	0.95	0.25	0.75
	Basis Func, *Φ*	Multi.	Multi.	T. P.	Multi.	Multi.	Multi.	Gauss	Inv. Multi.	Multi.	T.P.	Multi.
KR	U.B. *θ, c*	0.1	0.011	1	1	0.1	0.011	0.1	0.011	0.1	1	0.1
	L.B. *θ, b*	0.01	0.001	0.001	0.001	0.01	0.001	0.01	0.001	0.001	0.01	0.01
	Corr. Func.	Spline	Spher.	Exp.	Linear	Gauss.	Linear	Gauss.	Spher.	Gauss.	Spline	Spline
	Reg. Deg.	0	1	0	1	0	1	0	0	1	0	0
SVR	*c*	1	1	100	10	0.01	10	10	10	1	10	1
	Pen. Par., C	10	2	0.1	2	10	2	5	5	5	0.1	5

Multi. is Multiquadric, T.P. is Thin Plate, Inv is Inverse, Exp is Exponential and Spher is Spherical

Table 4.3 Tuned Metamodel Parameters for Mg

Magnesium		FFI				SIDE			OFI			
		Int Toe	Int Dash	Accel	Int Eng	Int Door	Accel	Int Eng	Int Toe	Int Dash	Accel	Int Eng
PRS	Poly. Degree	1	1	1	1	1	1	1	1	1	1	1
RBF	Parameter, *c*	0.05	0.05	0.2	0.05	1	1	1	1	0.15	0.05	1
	Basis Func., *Φ*	Gauss	Gauss	Multi.	Gauss.	Multi.	Inv. Multi.	Multi.	Multi.	Gauss	Multi.	Multi.
KR	U.B. *θ, c*	0.011	0.1	0.011	0.011	0.011	0.1	0.011	1	0.1	1	1
	L.B. *θ, b*	0.01	0.001	0.001	0.001	0.001	0.01	0.001	0.001	0.001	0.01	0.001
	Corr. Func.	Cubic	Gauss.	Spline	Exp.	Linear	Spline	Cubic	Spher.	Spline	Spline	Cubic
	Regr. Deg.	0	0	0	0	1	0	1	1	0	0	1
SVR	*c*	1	1	10	0.01	10	0.01	10	10	0.01	1	10
	Pen. Par., C	5	10	0.1	2	2	0.1	0.1	10	10	0.1	2

Multi. is Multiquadric, T.P. is Thin Plate, Inv is Inverse, Exp is Exponential, and Spher is Spherical

Single-Objective (SO) Optimization

Weight minimization is the objective of this optimization problem while maintaining or improving the baseline crash responses. Both the steel and magnesium models are used with each being compared to its own baseline responses. This is formulated as

$$\begin{aligned} \min \quad & F(x) = weight(x) \\ s.t. \quad & R_j \leq R_{jbase}; j = 1..8 \\ & R_j \geq R_{jbase}; j = 9..11 \\ & 0.5x_{base} \leq x \leq 1.5x_{base} \end{aligned} \tag{4.2}$$

where *F(x)* is the objective function, *x* is the input vector of 15 design variables (thickness), R_j is the *jth* response predicted by a metamodel, and R_{jbase} is the response of the baseline model (material specific). In Eq. (4.2), $j = 1..8$ represents the intrusion distances and accelerations and $j = 9..11$ represents the internal energy responses.

This problem was solved using Sequential Quadratic Programming (SQP) implemented in the VisualDOC[41] software package. Eight starting points were used because SQP is a gradient-optimization technique that can find local minima rather than global. Results are shown only from the best starting point. SQP approximates the original nonlinear problem by solving the quadratic programming sub-problem

$$\begin{aligned} min \quad & Q(d, X) = \nabla f(X)^T d + 0.5 d^T B d \\ s.t. \quad & \beta_j g_j(X) + \nabla g_j(X)^T d \leq 0 \quad j = 1, \dots, N_g \\ & \bar{\beta} h_m(X) + \nabla h_m(X)^T d = 0 \quad m = 1, \dots, N_h \end{aligned} \tag{4.3}$$

where d, is the search direction vector, X the design variable vector, B is positive definite matrix that approximates $\nabla^2 L$ (L is the Lagrangian), β_j and $\bar{\beta}$ are constants, g_j represents inequality constraints, h_m represents equality constraints, $N_g$is the number of inequality

constraints, and $N_{/\!/}$ is the number of equality constraints. Search direction vector $\boldsymbol{d}$ can be determined by using the Lagrange multiplier method with Lagrangian

$$\tilde{L}(d,\lambda) = Q + \sum_{j=1}^{N_g} \lambda_j \left(\beta_j g_j + \nabla g_j{}^T d + s_j^2 \right) + \sum_{m=1}^{N_h} \lambda_{N_g} + m(\bar{\beta} h_m + \nabla h_m^T d) \quad (4.4)$$

The design variable vector is updated using

$$X^{(k+1)} = X^{(k)} + \alpha_k^* d^{(k)} \quad (4.5)$$

where α_k^* is the optimal step size along the search direction found by minimizing the penalty function given by

$$\phi\left(X^{(k+1)}\right) = \phi(\alpha_k) = f(\alpha_k) + \sum_{j=1}^{N_g} \mu_j{}^{(k)} \{\max [0, g_j(\alpha_k)]\} + \sum_{m=1}^{N_h} \mu_{N_g}{}^{(k)} + m|h_m(\alpha_k)| \quad (4.6)$$

Total mass of the steel parts dropped from 105.2 kg to 88.0 kg and total mass of the magnesium parts dropped from 42.7 kg to 37.2 kg. That is a 16% and 13% reduction for steel and magnesium, respectively. Responses predicted by the metamodels during SQP optimization were compared to the LS-DYNA simulation results at the optimum point. Table 4.4 shows percent error of the metamodel predictions relative to the simulation results. Percent errors for steel were less than 5% for most responses and greater than 13% for the others. Magnesium percent errors were at or less than 10% except for OFI acceleration which was 23.3%. The total number of function calls for this solution, including all starting points, is 2,483 for steel in nine iterations and 2,095 for magnesium in nine iterations.

Table 4.4 Metamodel Prediction Error at the SO Optimums

		% from St LS-DYNA	% from Mg LS-DYNA
FFI	Int Toe	4.1%	4.9%
	Int Dash	13.8%	1.2%
	Accel	14.9%	3.0%
	Int Eng	3.1%	1.6%
SIDE	Int Door	4.4%	2.2%
	Accel	15.8%	1.9%
	Int Eng	2.9%	0.1%
OFI	Int Toe	5.1%	10.1%
	Int Dash	24.1%	6.7%
	Accel	0.4%	23.3%
	Int Eng	0.9%	1.8%

Figure 4.1 shows the normalized design variables at the SO optimums. Variable *x9* (left and right shotgun) went to the lower bound in both the Mg and St SO optimum designs. The variables that increased at the SO St optimum were the Outer Cabin and Inner Front rail (*x6* and *x11*). The Outer Cabin(s) is the most energy absorbing part for SIDE and one of the heaviest whereas the Inner Side Rail(s) is the most energy absorbing part for OFI and nearly the most for FFI. The part thicknesses that increased more than

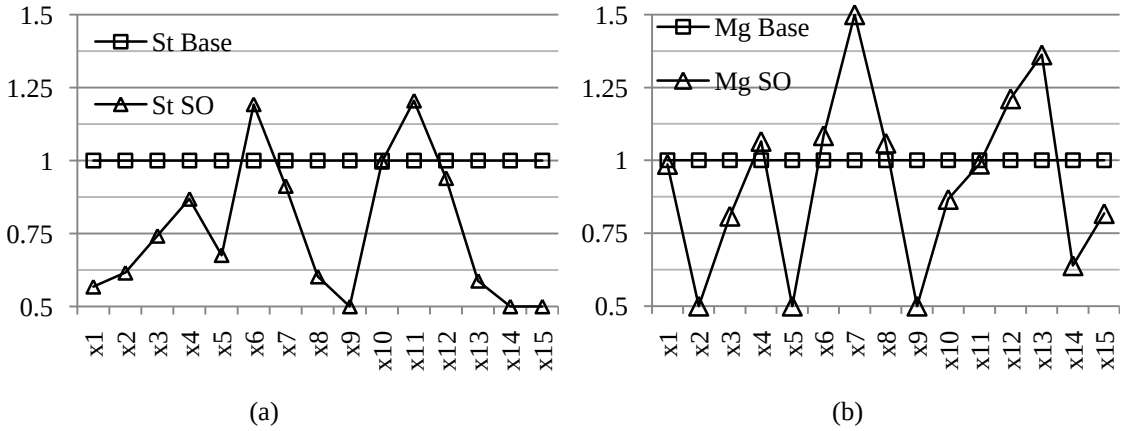

Figure 4.1 Normalized Design Variables for SO Optimums (a) St and (b) Mg

12% at the SO Mg optimum were the Cabin Seat Reinforcement (*x7*), Side Rail Extension(s) (*x12*), and the Rear Plate (*x13*). The part thicknesses that decreased to their lower bound were the Front Bumper (*x2*), Rear Cabin Floor (*x5*), and Shotgun(s) (*x9*).

Response values at the baseline and SO optimum points for both steel and magnesium can be found in Table 4.5 along with a percent difference relative to their respective baselines. It should be noted that these responses are the results from the LS-DYNA simulation at the optimum point found using the metamodels and not the metamodel predictions. The intrusion distances using the Mg parts are still significantly larger than the corresponding St parts except for intrusion at the dashboard for OFI. The accelerations are lower or about the same for Mg compared to St while internal energy is slightly lower.

Table 4.5 Crash Reponses at the SO Optimums

		St SO Opt	% from St Base	Mg SO Opt	% from Mg Base
FFI	Int Toe (mm)	170	8.0%	274	-7.1%
	Int Dash (mm)	108	-11.2%	167	-9.9%
	Accel (g's)	69.0	8.6%	53.1	7.8%
	Int Eng (kJ)	65.7	5.4%	60.1	-3.6%
SIDE	Int Door (mm)	333	6.2%	414	-1.2%
	Accel (g's)	38.6	-19.5%	41.2	1.0%
	Int Eng (kJ)	23.2	3.8%	21.5	0.3%
OFI	Int Toe (mm)	233	-14.7%	320	-8.4%
	Int Dash (mm)	269	9.1%	252	-34.8%
	Accel (g's)	36.6	4.4%	30.7	-15.0%
	Int Eng (kJ)	40.2	1.9%	38.3	-2.4%
MASS (kg)		88.0	-16.4%	37.2	-13.0%

Multi-Objective (MO) Optimization

Results in the previous section suggest that the magnesium designs, both baseline and SO optimum, maintain or improve upon the steel baseline responses for acceleration and internal energy but exceed the steel baseline intrusion distances. Another optimization problem is formulated and solved to determine the mass of a magnesium design that meets the crashworthiness of steel baseline.

This optimization problem uses the magnesium model and targets the baseline steel intrusion distance while constraining the acceleration and internal energy to the steel baseline values. Mass is not considered for this problem. This problem is formulated as

$$s.t. \quad \begin{array}{l} \text{target} \quad F(x) \\ R_j \le R_{jSt}; j = 6..8 \\ R_j \ge R_{jSt}; j = 9..11 \\ 0.5x_{Mg} \le x \le 1.5x_{Mg} \end{array} \tag{4.7}$$

where *F(x)* represents a composite objective function representing the intrusion distances of the baseline steel model, R_{jSt} for $j = 6..8$ are the baseline steel accelerations, R_{jSt} for $j = 9..11$ are the baseline steel internal energies, and $x_{Mg}$are the baseline magnesium design point values.

VisualDOC software is again used to solve this problem using SQP with eight starting points. Results from the best starting point are shown. Compromise programming was used inside VisualDOC to convert this multi-objective into a single-objective optimization problem. Using the compromise programming formulation, the composite objective function in Eq. (4.7) is given by

$$F(x) = \sum_{j=1}^{J} W_j \left[\frac{R_j(x) - {R_{jSt}}^{Target}(x)}{{R_{jMg}}^{Worst}(x) - {R_{jSt}}^{Target}(x)} \right]^2 \; j = 1..5 \tag{4.8}$$

where J is the number of targeted objective functions, W_j is the weight factor for the *j-th* objective, $R_j(x)$ is *j-th* objective, ${R_{jSt}}^{Target}(x)$ is the target value of the *j-th* objective, and ${R_{jMg}}^{Worst}(x)$ is the worst known value of the *j-th* objective (the responses at the initial magnesium design). The responses predicted by the metamodels and the LS-DYNA verified values at the MO optimum design point are found in Table 4.6. The metamodel errors are generally less than 10% with only two responses above 11%. The total number of function calls, including all starting points, is 2,909 in nine iterations.

Table 4.6 Metamodel (MM) Prediction Error at the MO Optimums

		Mg MO (MM)	Mg MO (LS- DYNA)	% from DYNA
FFI	Int Toe (mm)	166	186	-10.6%
	Int Dash (mm)	136	131	4.4%
	Accel (g's)	52.0	59.3	-12.3%
	Int Eng (kJ)	65.3	62.0	5.2%
SIDE	Int Door (mm)	328	361	-9.1%
	Accel (g's)	44.2	48.0	-8.0%
	Int Eng (kJ)	22.1	21.9	0.8%
OFI	Int Toe (mm)	256	212	20.7%
	Int Dash (mm)	247	236	4.7%
	Accel (g's)	35.0	37.0	-5.4%
	Int Eng (kJ)	39.0	37.9	2.7%

Figure 4.2 shows the normalized design variables for the Mg MO and Mg SO optimums. The Cabin Seat Reinforcement (*x7*) remained at its maximum allowed value with the Outer Cabin (*x6*), Side Rail Extension (*x12*), and Rear Plate (*x13*) also going to the maximum values. The Rear Cabin Floor (*x5*) went from its lower bound at Mg SO to nearly the upper bound at Mg MO. Shotgun thickness (*x9*) went to its lower bound.

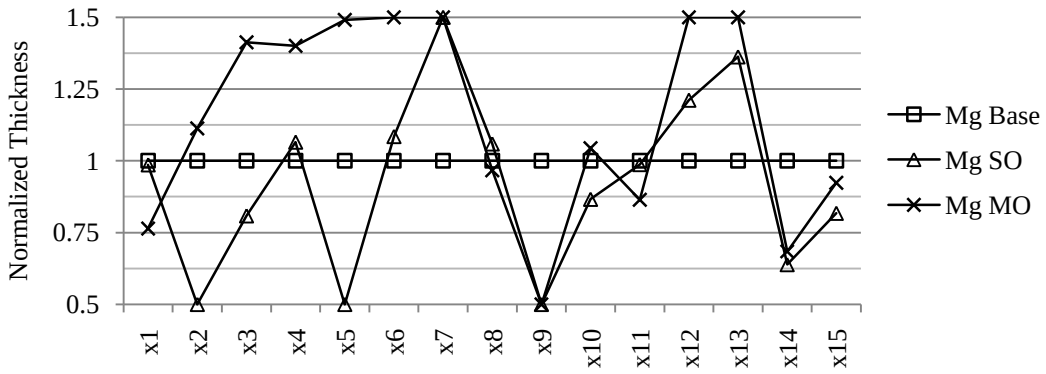

Figure 4.2 Normalized Design Variables for MO Optimums

The intrusion distances at the magnesium MO optimum show a reduction from the Mg baseline. These responses are also closer to the steel baseline, see Figure 4.3. One FFI intrusion distance is larger while the other is about the same as the St baseline, the SIDE intrusion distance is larger, and the OFI intrusions are both smaller than the St baseline. These values are the LS-DYNA simulation results at the MO optimum rather than the metamodel predictions. This design using the magnesium parts has a mass that is about 50% of the baseline steel design, 50.7 kg compared to 105.2 kg, and is 8 kg heavier than the baseline magnesium design.

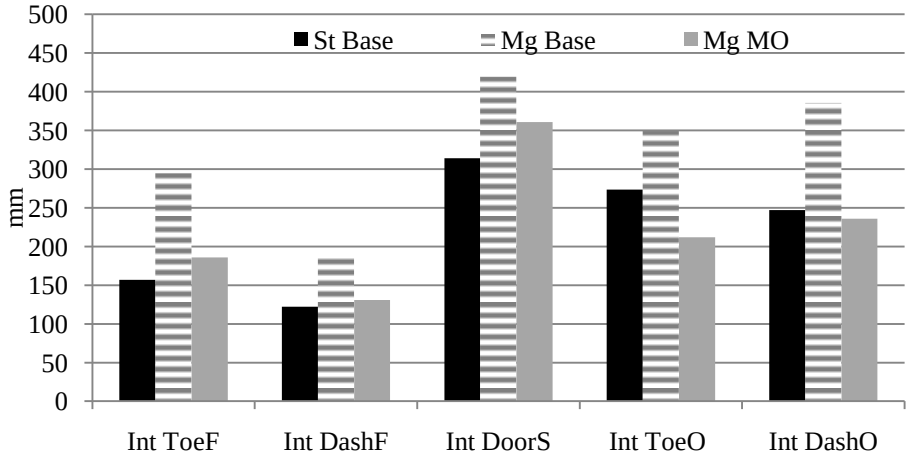

Figure 4.3 Intrusion Distance at the Baselines and MO Optimum; F is FFI, S is SIDE, and O is OFI

Results of the other responses of interest are found in Table 4.7 along with percentage comparisons with the Mg and St baselines. The acceleration responses are all larger than the Mg baseline but the same or smaller for FFI and SIDE compared to the St baseline. The internal energy response at the MO optimum are the same as the baselines for FFI, lower than the St baseline and higher than the Mg baseline for SIDE, and lower than both for OFI.

Table 4.7 Responses at MO Optimums

	FFI		SIDE		OFI		Mass
	Accel	Int Eng	Accel	Int Eng	Accel	Int Eng	
Mg MO…	59.3 g's	62.0 kJ	48.0 g's	21.9 kJ	37.0 g's	37.9 kJ	50.7 kg
…Relative to St Base	-6.6%	-0.4%	0.2%	-2.1%	5.6%	-3.7%	-51.8%
…Relative to Mg Base	20.5%	-0.5%	17.8%	2.3%	2.3%	-3.3%	18.7%

Optimization Results Summary

Optimization problems in this study focused on reducing mass and maintaining crash performance. Improved crashworthiness beyond the steel baseline was desirable but not an objective. Results show that the magnesium designs have lower mass than the steel designs and similar or better crashworthiness when considering acceleration and internal energy but worse if considering intrusion distance. The all steel model was 17.2 kg lighter when optimized for mass than the steel baseline model. The optimized model with selected parts replaced with magnesium was 54.5 kg lighter than the steel baseline and 37.3 kg lighter than the optimized steel model with similar crash responses. Response results for SO and MO optimizations are summarized in Figure 4.4.

Design variable values representing wall thickness of individual parts at the baseline and optimized designs can be found in Table 4.8. Shotgun thickness went to its lowest allowable value (50% lower than the baseline) for each of the three optimization problems solved. This suggests that this part may be at its limit for energy absorption within these thickness bounds because the shotgun has significant energy absorption for frontal impacts. Components such as the Roof (*x14*) were chosen for contributions to vehicle stiffness and provide little energy absorbing capability to the vehicle. The Roof thickness was significantly reduced in these designs as a result. Figures 4.5, 4.6, and 4.7 show simulation images of the five designs for FFI, SIDE, and OFI, respectively. Differences can be observed in the door for the FFI scenario, the door and roof for SIDE, and the roof for OFI.

Table 4.8 Design Variable Summary (thicknesses in mm)

Part	Part No.	Design Variable	St Base	Mg Base	St SO	Mg SO	Mg MO
A-Pillar	310,311	x_1	1.611	2.597	0.915	2.561	1.984
Front Bump	330	x_2	1.956	5.975	1.204	2.987	6.649
Firewall	352	x_3	0.735	1.072	0.545	0.867	1.515
Front Floor Panel	353	x_4	0.705	1.136	0.612	1.211	1.592
Rear Cabin Floor	354	x_5	0.706	1.138	0.477	0.569	1.696
Outer Cabin	355,356	x_6	0.829	1.366	0.988	1.482	2.049
Cabin Seat Reinf.	357	x_7	0.682	1.099	0.622	1.649	1.649
Cabin Mid Rail	358,359	x_8	1.050	1.692	0.633	1.792	1.636
Shotgun	373,374	x_9	1.524	3.620	0.762	1.810	1.810
Inner Side Rail	389,391	x_{10}	1.895	3.966	1.887	3.436	4.141
Outer Side Rail	390,392	x_{11}	1.522	3.186	1.834	3.145	2.754
Side Rail Exten.	398,399	x_{12}	1.895	3.966	1.780	4.805	5.950
Rear plate	415	x_{13}	0.710	1.144	0.417	1.559	1.717
Roof	416	x_{14}	0.702	1.157	0.351	0.739	0.791
Susp. Frame	439	x_{15}	2.606	5.342	1.303	4.367	4.931

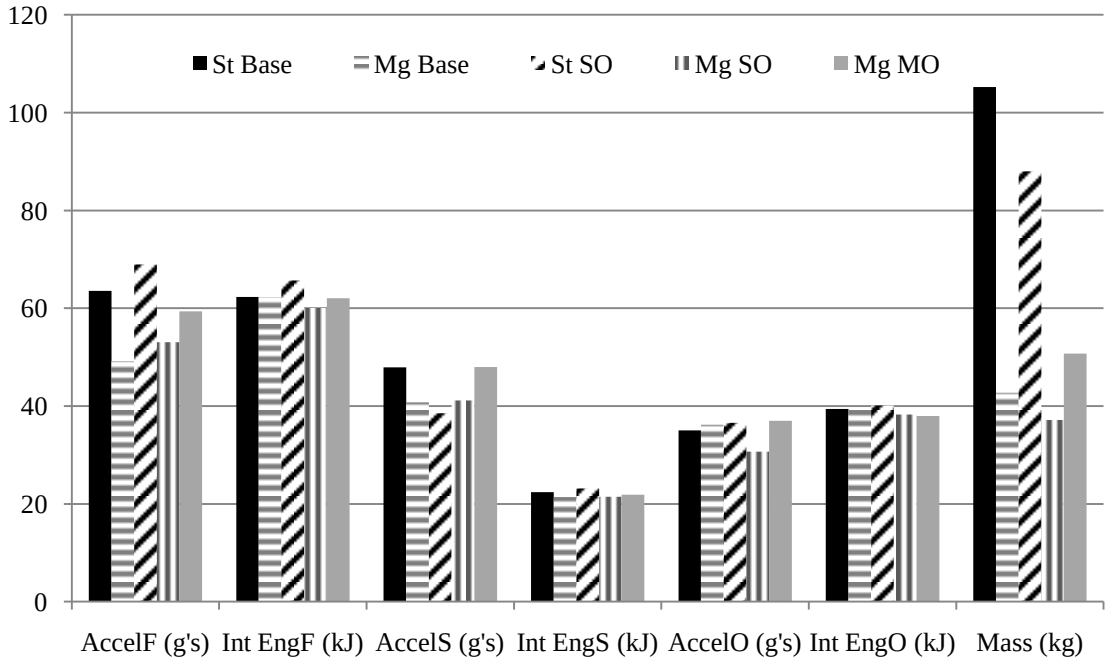

(a)

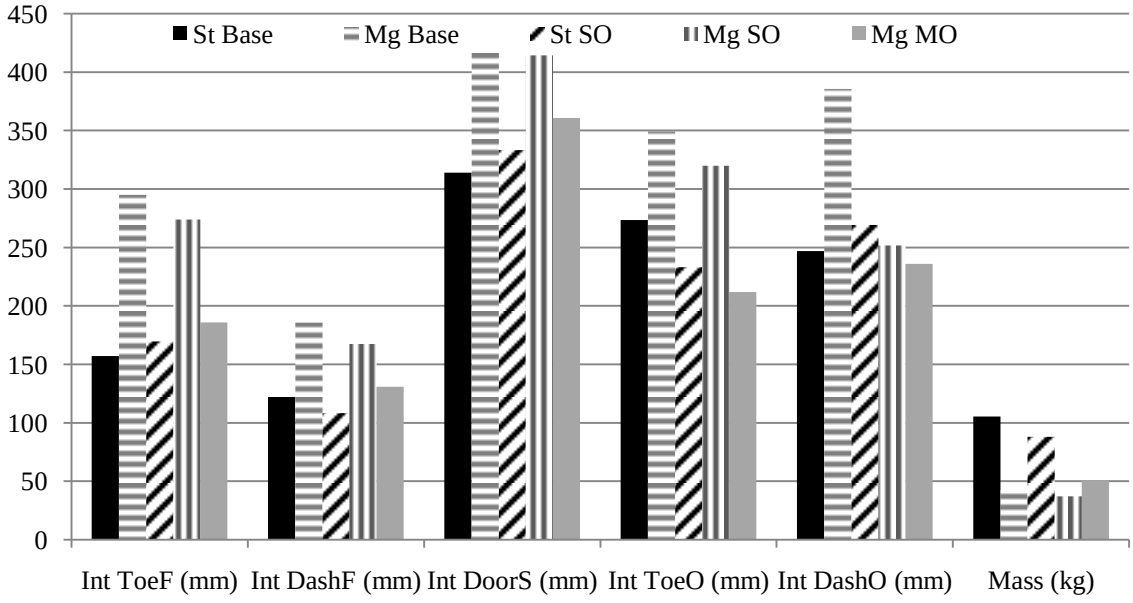

(b)

Figure 4.4 Optimization Response Results Summary for (a) Accelerations and Internal Energies and (b) Intrusion Distances; F is FFI, S is SIDE, and O is OFI

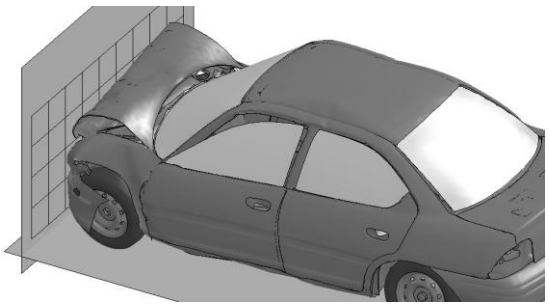

(a) FFI St Base

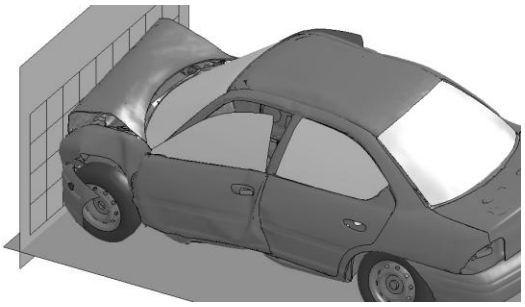

(b) FFI Mg Base

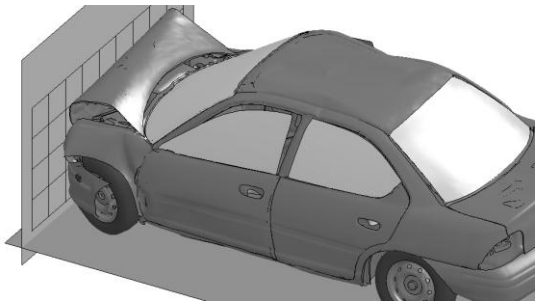

(c) FFI St SO

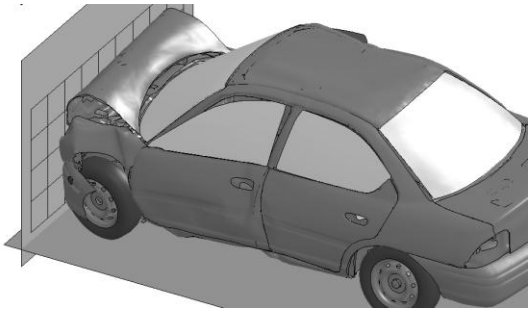

(d) FFI Mg SO

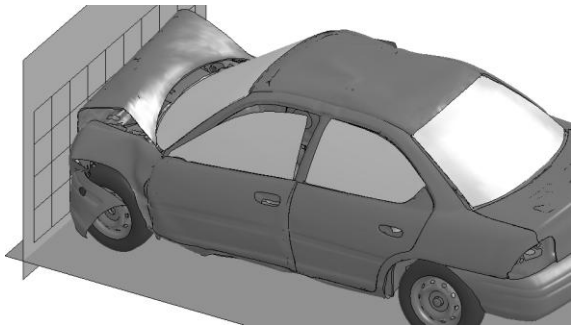

(e) FFI Mg MO

Figure 4.5 Simulation Images of the Designs, FFI at 150 ms

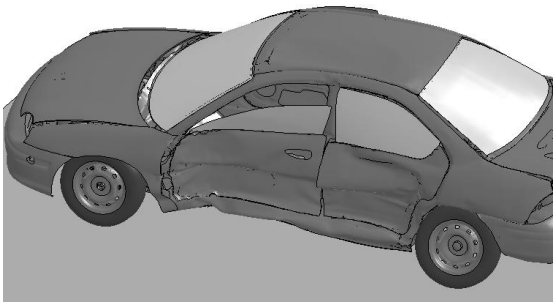

(a) SIDE St Base

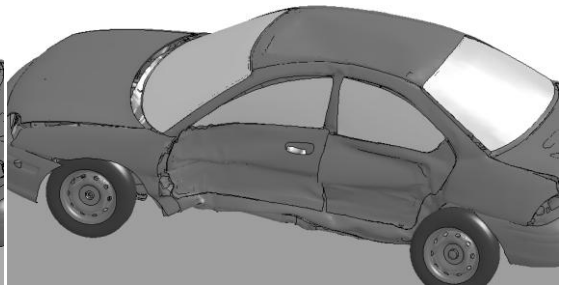

(b) SIDE Mg Base

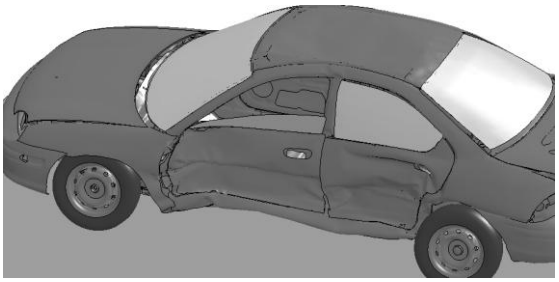

(c) SIDE St SO

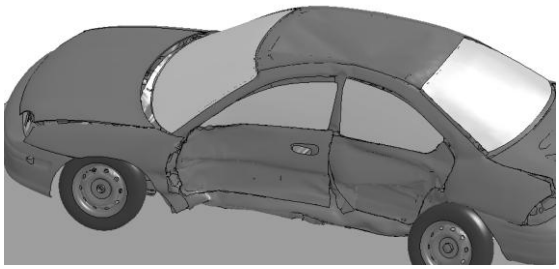

(d) SIDE Mg SO

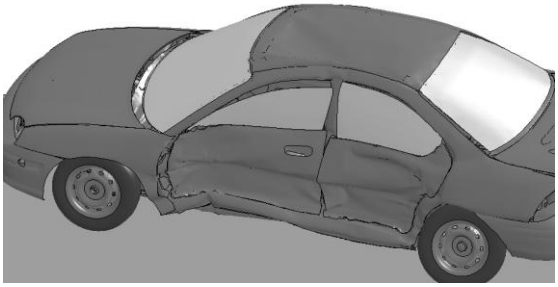

(e) SIDE Mg MO

Figure 4.6 Simulation Images of the Designs, SIDE at 150 ms

(a) OFI St Base

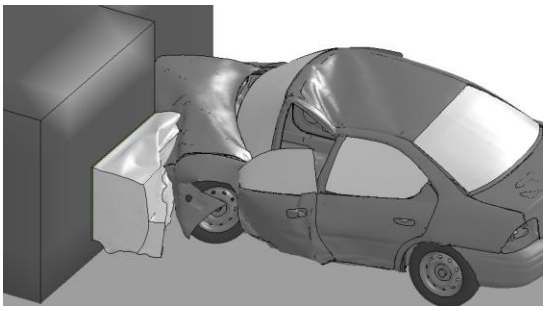

(b) OFI Mg Base

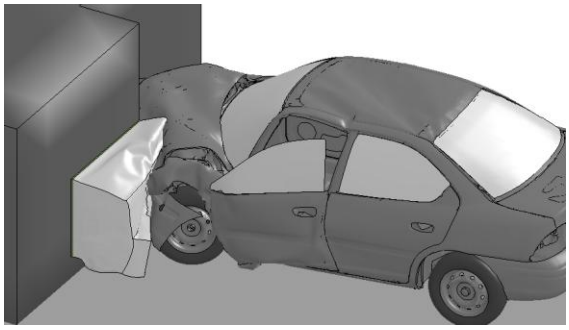

(c) OFI St SO

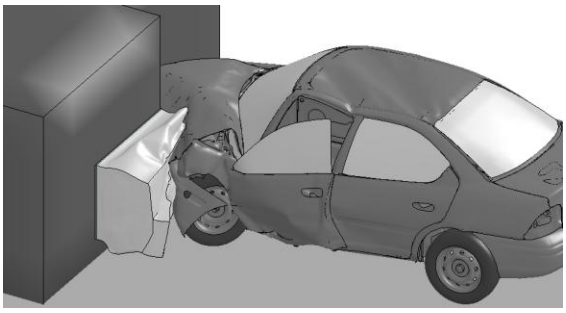

(d) OFI Mg SO

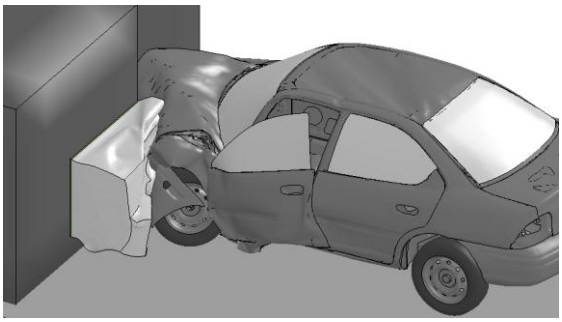

(e) OFI Mg MO

Figure 4.7 Simulation Images of the Designs, OFI at 150 ms

CHAPTER V

OPTIMIZATION WITH DUMMY MODEL

This chapter presents the optimization problem and results using the Dodge Neon FE models with the dummy and interior included. Only the SIDE dummy responses will be used in the optimization problem because of the poor results during validation of the FFI and OFI. Optimization problems in this chapter use the three SIDE dummy responses, rib deflection (Rib Def), maximum, resultant pelvic acceleration (Pelvis Accel), and Thoracic Trauma Index (TTI), total internal energy of the selected parts for FFI and SIDE (Int Eng and Int Eng), and intrusion distance at the toeboard for FFI (Int Dis Toe). All of these responses are taken from results of the model with the dummy. Total mass of the selected parts is the final responses considered for a total of seven. A metamodel is not constructed for mass.

The same DOE generated using Latin Hypercube Sampling in Chapter IV is used in this Chapter as well. Simulations at each of the forty-six DOE points were run for the FFI and SIDE scenarios. No OFI responses are included because of problems running the necessary DOE simulations. This gives a total of 184 simulations.

The overall objective of this optimization process is to find a design that minimizes weight but does not exceed the baseline response and the limits placed on occupant injury criteria by the Federal Motor Vehicle Safety Standards (FMVSS). Metamodel tuning results are discussed first followed by discussion of the optimization

problems. Part thicknesses discussed in Chapter III with the same baseline values and limits are used as design variables.

Metamodel Tuning Parameters

Metamodel tuning was performed using the same methods described in Chapter IV. An Optimized Ensemble was again created using the tuned base metamodels of the six responses by minimizing the GMSE of the ensemble. The weight factors of the optimized ensemble are shown in Table 5.1. Kriging and Support Vector Regression are the models making up the highest percentage of the ensembles similar to the metamodels built without using the dummy model. Radial Basis Function does not contribute to the ensembles for any St response. Table 5.2 and 5.3 show the tuned metamodel parameters for steel and magnesium, respectively.

Table 5.1 Optimized Ensemble Weight Factors (Dummy)

		FFI		SIDE			
		Int Eng	Int Dis Toe	Int Eng	Rib Def	TTI	Pelvis Accel
St	PRS	0	0	0	0	0.06	0
St	GP	0	0.29	0.02	0	0.68	0.2
St	RBF	0	0	0	0	0	0
St	KR	0.75	0.07	0.82	0.83	0.26	0.7
St	SVR	0.25	0.64	0.16	0.17	0	0.1
Mg	PRS	0	0	0	0	0	0
Mg	GP	0	0.3	0	0	0	0.17
Mg	RBF	0.07	0	0	0.015	0	0.11
Mg	KR	0.87	0.61	0.59	0.76	1	0.7
Mg	SVR	0.06	0.09	0.41	0.23	0	0.02

Table 5.2 Tuned Metamodel Parameters for St (Dummy)

		FFI		SIDE			
		Int Eng	Int Dis Toe	Int Eng	Rib Def	TTI	Pelvis Accel
PRS	Poly. Degree	1	1	1	1	1	1
RBF	Parameter, c	0.05	1	1	0.05	0.55	1
	Basis Func, Φ	Gauss	Multi	Multi	Gauss	Multi	Multi
KR	U.B. θ, c	0.011	0.011	0.1	0.011	0.1	0.1
	L.B. θ, b	0.001	0.01	0.01	0.001	0.01	0.01
	Corr. Func.	Spher	Cubic	Spline	Gauss	Spline	Gauss
	Reg. Deg.	1	0	0	0	0	0
SVR	c	0.01	0.01	10	0.01	10	10
	Pen. Par., C	0.1	2	2	2	2	10

Multi. is Multiquadric and Spher is Spherical

Table 5.3 Tuned Metamodel Parameters for Mg (Dummy)

		FFI		SIDE			
		Int Eng	Int Dis Toe	Int Eng	Rib Def	TTI	Pelvis Accel
PRS	Poly. Degree	1	1	1	1	1	1
RBF	Parameter, c	0.05	1	1	0.65	1	1
	Basis Func, Φ	Guass	Multi	Multi	Multi	Multi	Multi
KR	U.B. θ, c	0.1	0.011	1	0.011	0.1	0.011
	L.B. θ, b	0.01	0.001	0.001	0.01	0.001	0.01
	Corr. Func.	Guass	Cubic	Exp	Spher	Spher	Cubic
	Reg. Deg.	0	1	0	0	0	0
SVR	c	10	10	0.01	10	10	0.01
	Pen. Par., C	10	10	10	0.1	2	2

Multi. is Multiquadric, Gauss is Gaussian, Exp is Exponential and Spher is Spherical

Single-Objective (SO1) Optimization with Baseline Constraints

Weight minimization is the objective of this optimization problem while maintaining or improving upon the baseline responses. Both of the steel and magnesium models are used with each being compared to its own baseline responses. This is formulated as

$$\begin{aligned} \min \quad & F(x) = weight(x) \\ s.t. \quad & R_j \leq R_{jbase}; j = 1..4 \\ & R_j \geq R_{jbase}; j = 5..6 \\ & 0.5x_{base} \leq x \leq 1.5x_{base} \end{aligned} \tag{5.1}$$

where *F(x)* is the objective function, *x* is the input vector of 15 design variables, R_j is the *jth* response predicted by a metamodel, and R_{jbase} is the response of the baseline model (material specific). In Eq. (5.1), $j = 1..4$ is the toeboard intrusion distance, rib deflection, TTI, and pelvic acceleration while $j = 5..6$ represents the internal energy responses.

This problem was solved using SQP in VisualDOC using six starting points. Total mass of the steel parts dropped from 105.2 kg to 98.3 kg. That is a 6.6% reduction. Responses predicted by the metamodels during optimization were compared to LS-DYNA simulation results at the optimum point. Table 5.4 shows percent error of the metamodel predictions relative to the simulation results. Percent error for steel was around 5% or lower except for Rib Deflection and Toeboard Intrusion. Magnesium responses were all at or below 3% except maximum pelvis acceleration which was 7.6%. The total number of function calls for this solution, including all starting points, is 1,752 for steel in seven iterations and 443 for magnesium in eleven iterations.

Table 5.4 Metamodel Prediction Error at the SO1 Optimums

		St SO1 MM	St DYNA	St % from DYNA	Mg SO1 MM	Mg DYNA	Mg % from DYNA
FFI	Int Eng (kJ)	60.60	57.65	5.12%	61.00	62.8	-2.87%
	Int Dis Toe (mm)	130.90	114.02	14.80%	224.78	229.16	-1.91%
SIDE	Int Eng (kJ)	19.14	19.14	0.00%	18.61	19.2	-3.10%
	Rib Def (mm)	42.23	37.61	12.28%	44.47	43.32	2.65%
	TTI (g's)	60.97	61.32	-0.57%	67.75	68.36	-0.90%
	Pelvis Accel (g's)	75.85	77.37	-1.96%	60.87	65.88	-7.60%

Figure 5.1 shows the normalized design variables at the SO1 optimums. Roof (*x14*) and Suspension Frame (*x15*) went to the lower bound while Side Rail Extension went to its upper bound for the steel SO1 design. None of the design variables reached the lower bound for magnesium but Front Bumper (*x2*), Rear Cabin Floor (*x5*), and Suspension Frame (*x15*) came close. Cabin Mid Rail (*x8*) and Outer Side Rail(*x11)* came close to the upper bound.

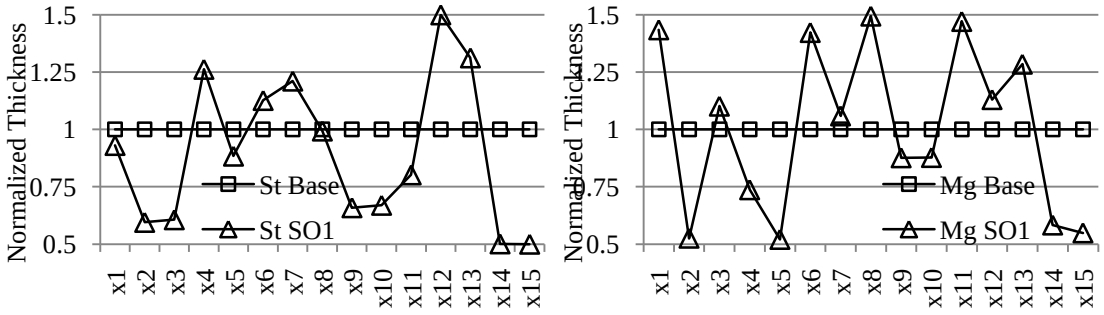

(a) (b)

Figure 5.1 Normalized Design Variables for SO1 Optimums (a) St and (b) Mg

Response values at the baseline and SO1 optimum points for both steel and magnesium can be found in Table 5.5 along with a percent difference relative to their

respective baselines. It should be noted that these responses are the results from the LS-DYNA simulation at the optimum point found using the metamodels and not the metamodel predictions. Steel responses except internal energy FFI improved their crash response or stayed the same at the SO1 optimum. All of the magnesium responses improved their crash performance except for TTI.

Table 5.5 Crash Reponses at the SO1 Optimum

		St SO1 opt	% from St Base	Mg SO1 opt	% from Mg Base
FFI	Int Eng	60.60	-5.06%	62.8	2.98%
	Int Dis Toe	130.90	-12.78%	229.16	-8.63%
SIDE	Int Eng	19.14	-0.10%	19.2	5.84%
	Rib Def	42.23	-11.00%	43.32	-3.50%
	TTI	60.97	0.80%	68.36	5.56%
	Pelvis Accel	75.85	-6.43%	65.88	-15.32%
	Mass (kg)	98.28	-6.60%	41.42	-3.00%

Single-Objective (SO2) Optimization with FMVSS Limit Constraints

An optimization problem is now formulated and solved using the FMVSS limits as constraints rather than baseline design values. The same responses are used for this problem. The objective is to find the lightest design that does not violate the FMVSS limits on the SIDE occupant responses. FFI part internal energy and intrusion distance at the toeboard as well as SIDE part internal energy are constrained to be the same or better than their baseline since there is no FMVSS limit on these responses. The SO2 problem is

$$\begin{aligned} \min \quad & F(x) = weight(x) \\ s.t. \quad & R_j \le R_{jFMVSS}; j = 1..3 \\ & R_j \le R_{jbase}; j = 4 \\ & R_j \ge R_{jbase}; j = 5..6 \\ & 0.5x_{base} \le x \le 1.5x_{base} \end{aligned} \tag{5.2}$$

where *F(x)* is the objective function, *x* is the input vector of 15 design variables, R_j is the *jth* response predicted by a metamodel, R_{jFMVSS} is the FMVSS limit on the SIDE occupant responses, and R_{jbase} is the response of the baseline model (material specific). In Eq. (5.2), $j = 1..3$ is the rib deflection, TTI, and pelvic acceleration, $j = 4$ is the toeboard intrusion distance, and $j = 5..6$ represents the internal energy responses.

SQP in VisualDOC is used to solve this problem using six starting points for steel and ten for magnesium. Total mass of the steel parts dropped from 105.2 kg to 94.24 kg and from 42.7 kg to 32.2 kg for magnesium. That is a 10.4% and 24.5% reduction for St and Mg, respectively. Metamodel prediction error compared to simulation results at the optimum point is shown in Table 5.6. Percent errors for steel were at or below 5% but higher overall for magnesium. Magnesium rib deflection had an error of 19.3% and toeboard intrusion had an error of 6.88%. Other magnesium responses had an error less than 6%. The total number of function calls for this solution, including all starting points, is 1,178 for steel in seven iterations and 638 for magnesium in seven iterations.

Table 5.6 Metamodel (MM) Prediction Error at the SO2 Optimums

		St SO2 (MM)	St SO2 (DYNA)	St % from (DYNA)	Mg SO2 (MM)	Mg SO2 (DYNA)	Mg % from (DYNA)
FFI	Int Eng (kJ)	61.42	59.63	3.00%	60.95	59.65	2.18%
	Int Dis Toe (mm)	131.02	137.96	-5.03%	249.68	233.6	6.88%
SIDE	Int Eng (kJ)	19.10	19.18	-0.42%	18.15	17.83	1.79%
	Rib Def (mm)	43.91	45.78	-4.08%	43.38	36.35	19.34%
	TTI (g's)	66.56	67.19	-0.94%	73.98	78.36	-5.59%
	Pelvis Accel (g's)	84.61	82.63	2.40%	87.05	89.61	-2.86%

Normalized design variables for the steel and magnesium design can be seen in Figure 5.2. Seven of the steel design variables reached the lower bound for the SO2

optimum. These were A-pillar(s) (*x1*), Front Bumper (*x2*), Firewall (*x3*), Cabin Seat Reinforcement (*x7*), Inner Side Rail (*x10*), Rear Plate (*x14*), and Suspension Frame (*x15*). Cabin Mid Rail (*x8*) and Side Rail Extension (*x12*) increased to their maximum values. For Magnesium the Shotgun(s) (*x9*), Roof (*x14*), and Suspension Frame (*x15*) all went to the lower bound while reached the upper bound. Cabin Mid Rail (*x8*) and Side Rail Extension (*x12*) were the largest relative increase in thickness.

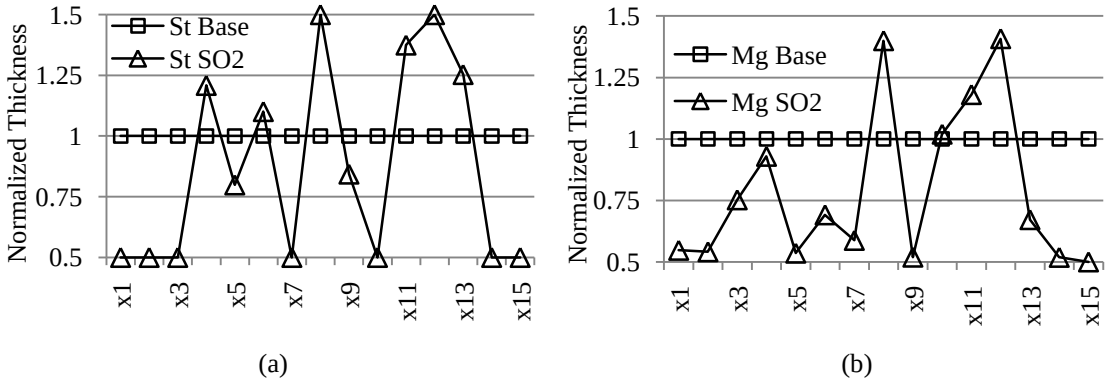

(a) (b)

Figure 5.2 Normalized Design Variables for SO2 Optimums (a) St and (b) Mg

Responses for SO2 optimum can be seen in Table 5.7 and are compared to the baseline response values. All St responses got worse except SIDE Internal Energy and

Table 5.7 Crash Reponses at the SO2 Optimums

		St SO2 opt	% from St Base	Mg SO2 opt	% from Mg Base
FFI	Int Eng	59.63	-1.80%	59.65	-2.18%
	Int Dis Toe	137.96	5.54%	233.6	-6.86%
SIDE	Int Eng	19.18	0.10%	17.83	-1.71%
	Rib Def	45.78	8.33%	36.35	-19.02%
	TTI	67.19	10.45%	78.36	21.00%
	Pelvis Accel	82.63	-0.07%	89.61	15.18%
Mass (kg)		94.24	-10.44%	32.2	-24.59%

Pelvis Acceleration which remained the same. Both rib deflection and toeboard intrusion for the magnesium design decreased while both TTI and pelvis acceleration increased. Both internal energy responses decreased from the baseline value.

Optimization Results Summary

SIDE occupant-based responses along with SIDE internal energy and FFI internal energy and toeboard intrusion distance were used as responses. Single objective optimizations were performed to minimize the weight of the vehicle while maintain the baseline crashworthiness (SO1) and then staying below the limits specified in the FMVSS for occupant-based responses (SO2).

Mass was reduced from 105.23 kg to 98.28 kg for the SO1 case and 94.24 kg for the SO2 case using the steel components. Magnesium designs saw a mass reduction from 42.7 kg to 41.42 for the SO1 case and 32.2 kg for the SO2 case. Table 5.8 shows the

Table 5.8 Design Variable Summary (Dummy) (thicknesses in mm)

Part	Design Variable	St Base	Mg Base	St SO1	St SO2	Mg SO1	Mg SO2
A-Pillar	x_1	1.611	2.597	1.499	0.806	3.725	1.422
Front Bump	x_2	1.956	5.975	1.164	0.978	3.138	3.233
Firewall	x_3	0.735	1.072	0.446	0.368	1.181	0.807
Front Floor Panel	x_4	0.705	1.136	0.89	0.852	0.837	1.056
Rear Cabin Floor	x_5	0.706	1.138	0.624	0.564	0.592	0.610
Outer Cabin	x_6	0.829	1.366	0.934	0.912	1.944	0.945
Cabin Seat Reinf	x_7	0.682	1.099	0.826	0.341	1.164	0.646
Cabin Mid Rail	x_8	1.050	1.692	1.043	1.575	2.529	2.368
Shotgun	x_9	1.524	3.620	1.004	1.285	3.171	1.880
Inner Side Rail	x_{10}	1.895	3.966	1.269	0.948	3.480	4.043
Outer Side Rail	x_{11}	1.522	3.186	1.221	2.092	4.686	3.760
Side Rail Exten.	x_{12}	1.895	3.966	2.843	2.843	4.482	5.583
Rear plate	x_{13}	0.710	1.144	0.932	0.890	1.470	0.769
Roof	x_{14}	0.702	1.157	0.352	0.351	0.674	0.600
Susp. Frame	x_{15}	2.606	5.342	1.303	1.303	2.930	2.672

values of the design variables at each of the optimum points found in this Chapter. Shotgun (*x9*) thickness was reduced or was at the lower bound just as in Chapter IV suggesting the part may be at its energy absorption capacity in these bounds. This may also be true for the Suspension Frame (*x15*). Components such as the Roof (*x14*) were chosen for contributions to vehicle stiffness and provide little energy absorbing capability to the vehicle. The Roof thickness was significantly reduced in these designs as a result.

The SO optimum designs found in Chapter IV were input into the SIDE dummy model to determine what the dummy-based injuries would be using the SO optimum found using vehicle-based responses. These results can be seen in Figure 5.3 with the SIDE occupant-based responses for each of the designs as well as the FMVSS limits on each; mass is also shown for comparison.

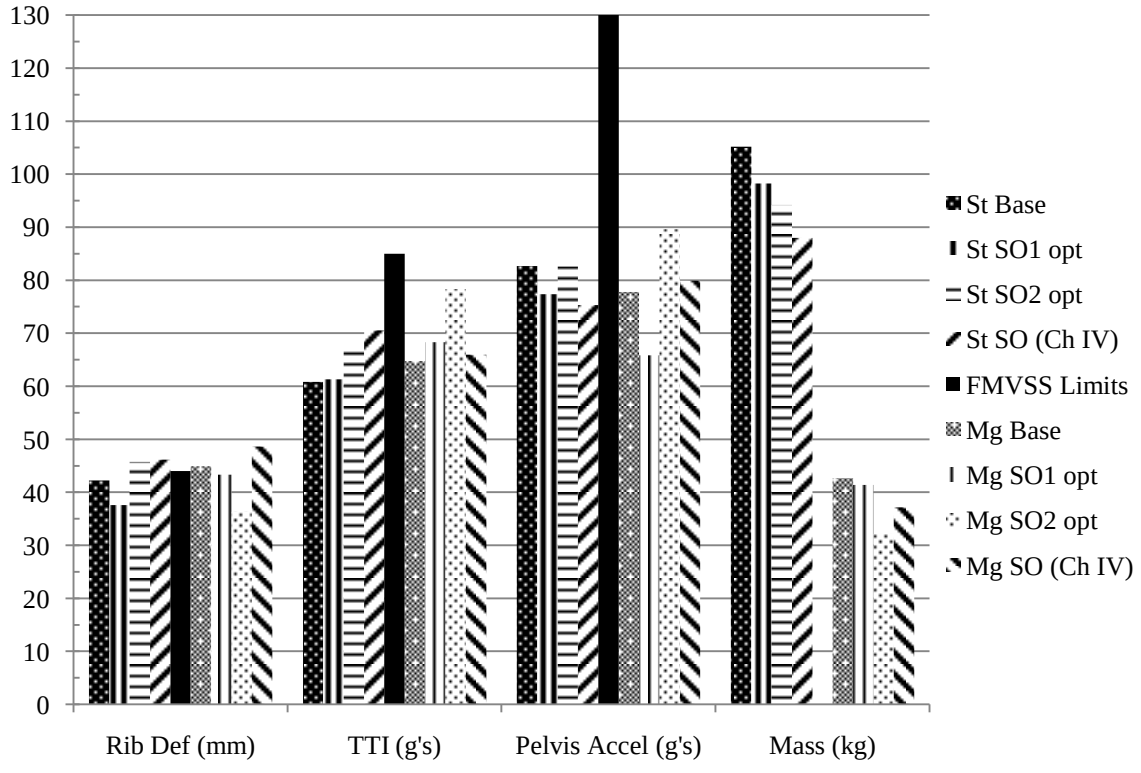

Figure 5.3 SIDE Occupant-Based Responses and the FMVSS Limits

Rib deflection was larger for the SO (Ch IV) design compared to the designs found in this chapter and exceeds the FMVSS limit for both materials. Magnesium TTI at SO (Ch IV) was larger than SO1 and SO2 and none of the designs exceeded the FMVSS limit. Maximum pelvis acceleration for steel was lowest in the SO1 (Ch IV) design. The lowest mass for the steel designs was the SO1 (Ch IV) and SO2 for magnesium.

Figure 5.4 shows percent change from the baseline responses of the SIDE responses for the six single-objective designs. This figure shows that in general the vehicle-based responses (intrusion distance at the door and acceleration at the middle of the B-pillar) do not indicate the same percentage change in injury as the dummy-based responses. Caution should be used when relying on door intrusion distance and maximum acceleration at the B-pillar to estimate injury.

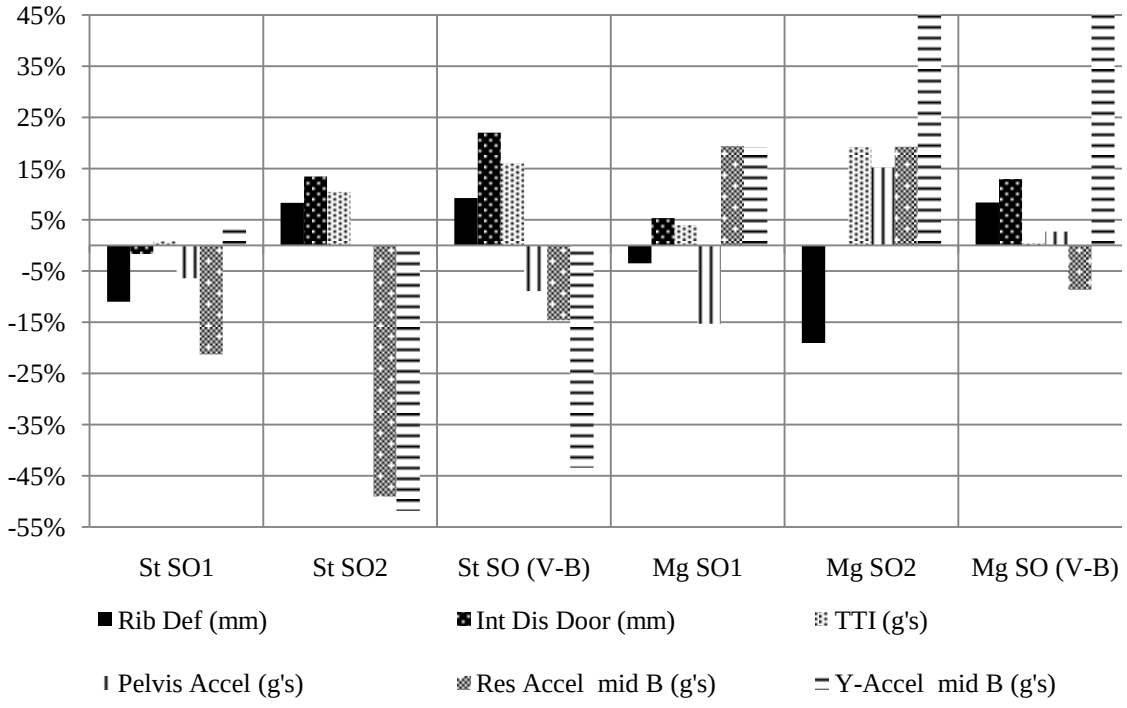

Figure 5.4 Percent Change from Baseline for Vehicle and Dummy Responses.

MG SO2 y-accel is 163.7% and MG SO (V-B) y-accel is 84.6%.

CHAPTER VI

CONCLUSIONS AND FUTURE WORK

This thesis used metamodeling and optimization techniques to explore the application of a lightweight magnesium alloy for a group of energy absorbing parts in a full vehicle model. Studies with and without a dummy model were performed.

A full-scale Dodge Neon model developed and validated for Full Frontal Impact (FFI) at the National Crash Analysis Center (NCAC) was incorporated into Side Impact (SIDE) and Offset Frontal Impact (OFI) scenarios without a dummy model. A SIDE impact model was then validated with a dummy model.

Vehicle-based responses from these three scenarios along with selected part mass were used as constraints and objectives during design optimization with part thicknesses as the design variables. Occupant-based responses from the SIDE model were then included. All crash simulations were performed using LS-DYNA finite element solver.

AZ 31 magnesium alloy was used to replace the baseline steel material in the finite element model. Due to the complexity of the failure characteristics of magnesium a limit on maximum plastic strain was used as a failure criterion to disable failed elements. This material substitution coupled with design optimization reduced the mass of the vehicle by approximately 50% of the baseline steel model and maintained or improved the crashworthiness for most of the factors considered using the model without the dummy. A direct substitution of magnesium for steel using thicknesses defined by

maintaining the internal energy absorption does not give the same crash characteristics or responses as the steel components.

Material substitution can change the deformation mode and folding mechanism of energy absorbing parts under crash loading as indicated by similar internal energies but significantly larger intrusion distances for the models using steel and magnesium components. Modification of the cross-sectional geometry as well as other geometric attributes should be considered along with the thickness modifications in vehicle design optimization using magnesium alloys.

Dummy-based optimum designs did not show as much of a percentage weight decrease as the vehicle-based optimum designs. The single-objective designs for steel and magnesium found using vehicle-based responses were compared to the single-objective designs found using SIDE dummy-based designs. Vehicle-based designs were simulated using the SIDE dummy model. Results show that using vehicle-based design responses may be acceptable for some cases but vehicle-based responses do not show the same percentage change between multiple designs compared to dummy-based responses.

Shotgun part thickness was reduced to the lower bound in all of the optimum designs. This suggests that this part is at its energy absorbing limit for these bounds and increasing part thickness does not necessarily increase energy absorption. This behavior was also seen to a lesser extent with the Suspension Frame. Parts such as the Roof were chosen as design parts primarily because of their contributions to vehicle stiffness. Roof thickness was significantly reduced in all of the designs because of its small contribution to energy absorption. Inclusion of vehicle stiffness responses during optimization would likely show less weight reduction in the optimized designs.

Future work will consider inclusion of vehicle stiffness (as a measure of overall rigidity as well as the noise, vibration, and harshness (NVH) characteristic of the vehicle) in the design optimization process, improving the accuracy of the vehicle models for frontal impact with a dummy model included, adding a microstructure-based material model to provide a more representative model of magnesium, and using alternative optimization strategies.

REFERENCES

[1] "Annual Progress Reports," Vehicle Technologies Program, http://www1.eere.energy.gov/vehiclesandfuels/resources/fcvt_reports.html. Mar 2011.

[2] "Magnesium Vision 2020: A North American Automotive Strategic Vision for Magnesium," United States Automotive Materials Partnership, 2006.

[3] Akkerman, A., Burger, M., Kuhn, B., Rajic, H., Stander, N., Thyagarajan, R., "Shape Optimization Of Instrument Panel Components For Crashworthiness Using Distributed Computing," Proceedings of the 6th International LS-DYNA Conference, Detroit, MI, 2000.

[4] Rais-Rohani, M., Solanki, K., Acar, E., and Eamon, C., "Shape and Sizing Optimization of Automotive Structures with Deterministic and Probabilistic Design Constraints," *International Journal of Vehicle Design*, Vol. 54, No. 1, 2010, pp. 309-338.

[5] Jung, D., Gea, HC., "Topology optimization of nonlinear structures," *Finite Elements in Analysis and Design*, Vol. 40, 2004, pp. 1417-1427.

[6] Mozumder, C., Bandi, P., Patel, N., Renaud, J., "Thickness based Topology Optimization for Crashworthiness Design using Hybrid Cellular Automata," Proceedings of the 12th AIAA/ISSMO Multidisciplinary Analysis and Optimization Conference, Victoria, British Columbia, Canada, Sept. 10-12, 2008.

[7] Rouhi, M., and Rais-Rohani, M., "Topology Optimization of Continuum Structures Using Element Exchange Method," Proceedings of the 4th AIAA Multidisciplinary Design Optimization Specialists Conference, Schaumburg, IL, Apr. 7-10, 2008.

[8] Fang, H., Rais-Rohani, M., Liu, Z. Horstemeyer, M.F. "A comparative study of metamodeling methods for multiobjective crashworthiness optimization," *Computers and Structures*, Vol. 83, 2005, pp. 2121-2136.

[9] Fang, H. Solanki, K, Horstemeyer, M.F., Rais-Rohani, M. "Multi-impact Crashworthiness Optimization with Full-scale Finite Element Simulations," Proceedings of the 6th World Congress of Computational Mechanics, Beijing, China, Sept. 5-10, 2004.

[10] Liao, X. Li, Q. Yang, X. Li, W. Zhang, W. "A two-stage multi-objective optimization of vehicle crashworthiness under frontal impact," *International Journal of Crashworthiness*, Vol. 13, No. 3, 2008, pp. 279-288.

[11] Sobieszczanski-Sobieski, J., Kodiyalam, S., Yang, R.Y., "Optimization of car body under constraints of noise, vibration, and harshness (NVH), and crash," *Structural and Multidisciplinary Optimization*, Vol. 22, 2001, pp. 298-306.

[12] Federal Motor Vehicle Safety Standards and Regulations. US Department of Transportation, National Highway Safety Administration. Washington, DC, 1998.

[13] Noureddine, A., Eskandarian, A., Digges, K., "Computer Modeling and Validation of a Hybrid III Dummy for Crashworthiness Simulation," *Mathematical and Computer Modeling*, Vol. 35, 2002, pp. 885-893.

[14] Silvestri, C. and Ray, M.H., "Development of a finite element model of the knee-thigh-hip of a 50th percentile male including ligaments and muscles," *International Journal of Crashworthiness*, Vol. 14, No. 2, 2009, pp. 215-229.

[15] Horstemeyer, M.F., Ren, X.C., Fang, H., Acar, E., and Wang P.T., "A comparative study of design optimization methodologies for side-impact crashworthiness using injury-based versus energy-based criterion," *International Journal of Crashworthiness*, Vol. 14, No. 2, 2009, pp. 125-138.

[16] Pan, F., Zhu, P., Zhang, Y., "Metamodel-based lightweight design of B-pillar with TWB structure via support vector regression," *Computers and Structures*, Vol. 88, 2010, pp 36-44

[17] Yang, R.J., Wang, N., Tho, C.H., Bobineau, J.P., Wang, B.P., "Metamodeling Development for Vehicle Frontal Impact Simulation," *Journal of Mechanical Design*, Vol. 127, 2005, pp. 1014-1020.

[18] Fang, H. and Wang, Q., "On the effectiveness of assessing model accuracy at design points for radial basis functions," *Communications in Numerical Methods in Engineering*, Vol. 24, 2008, pp. 219-235.

[19] Turner, C., "Design Space Analysis with Hyperdimensional Metamodels," Proceedings of the NSF Engineering Research and Innovation Conference, Honolulu, HI, 2009.

[20] Jin, R., Chen, W., and Simpson, T.W., "Comparative Studies of Metamodeling Techniques under Multiple Modeling Criteria," 2000, AIAA-2000-4801.

[21] Wang, L. Beeson, D. Wiggs, G. Rayasam, M. "A Comparison Of Meta-modeling Methods Using Practical Industry Requirements," Proceedings of the 47th

AIAA/ASME/ASCE/AHS/ASC Structures, Structural Dynamics, and Materials Conference. Newport, RI, 2006.

[22] Acar, E. and Rais-Rohani, M. "Ensemble of Metamodels with Optimized Weight Factors, *"Structural and Multidisciplinary Optimization,* Vol. 37, No. 3, 2008, pp. 279-294.

[23] Acar, E. and Solanki, K. "Improving the accuracy of vehicle crashworthiness response predictions using an ensemble of metamodels," *International Journal of Crashworthiness*, Vol. 14, No. 1, 2009, pp. 49-61.

[24] MATLAB: The Language of Technical Computing, Software Package, Ver. 7.8.0347 (R2009a), The Mathworks, Inc., 2009.

[25] Rasmussen, C., Williams, C. "Gaussian Processes for Machine Learning," MIT, Cambridge, Massachusetts, 2006.

[26] Lophaven SN, Nielsen HB, Søndergaard J "DACE – A MATLAB Kriging Toolbox," *Informatics and mathematical modeling*, Technical University of Denmark, Lyngby, 2002.

[27] Simpson, T. Mauer, T. Korte, J. Mistree, F. "Kriging Models for Global Approximations in Simulation-Based Multidisciplinary Design Optimization,"*AIAA Journal*, Vol. 39, No. 12, 2001, pp. 2231-2241.

[28] Cherkassky, V., Ma, Y. "Practical selection of SVM parameters and noise estimation for SVM regression," *Neural Networks*, Vol. 17, 2004, pp. 113-126.

[29] Gunn, SR. "Support vector machines for classification and regression," Technical Report, University of Southampton, 1997.

[30] Hsu, CW., Chang CC., Lin CJ. "A Practical Guide to Support Vector Classification," National Taiwan University, last updated 2010.

[31] Clarke, S., Griebsch, J., Simpson, T. "Analysis of Support Vector Regression for Approximation of Complex Engineering Analyses," *Journal of Mechanical Design*, Vol. 127, November, 2005, pp. 1077-1087.

[32] "Finite Element Model Archive," National Crash Analysis Center, http://www.ncac.gwu.edu/vml/models.html. June 2011.

[33] "LS-DYNA Keyword User's Manual: Volume II Material Models," Livermore Software Technology Corporation, Version 971, 2007, pp. 110-114 and 473-475.

[34] "Finite Element Model of Dodge Neon: Model Year 1996 Version 7," FHWA/NHTSA National Crash Analysis Center, 2006.

[35] "Saftey Compliance Testing for FMVSS 214 'Side Impact Protection – Passenger Cars':1997 Dodge Neon," U.S. Department of Transportation, prepared by MGA proving Grounds, Report no. 214-MGA-97-13, 1997.

[36] "National Highway Traffic Safety Administration Frontal Barrier Forty Percent Offset Impact Test: 1996 Dodge Neon," U.S. Department of Transportation, prepared by Karco Engineering, Report no. KAR-97-13,1997.

[37] "New Car Assessment Program (NCAP) Frontal Barrier Impact Test: 1996 Dodge Neon," U.S. Department of Transportation, prepared by Transportation Research Center Inc., Report no. TRC-96-N02, 1995

[38] Leiva, J.P., Wang, L., Recek, S., and Watson, B.C., "Automobile Design Using the *GENESIS* Structural Optimization Program," Proceedings of Nafems Seminar: Advances in Optimization Technologies for Product Design, Chicago, IL, Oct. 2001.

[39] "LSTC – LS-DYNA Finite Element Models," Livermore Software Technology Corporation, http://www.lstc.com/models/, June 2011.

[40] Wagner, D.A., Logan, S.D., Wang, K., Skszek, T., "FEA Predictions and Test Results from Magnesium Beams in Bending and Axial Compression," Proceedings of the SAE 2010 World Congress & Exhibition, Detroit, MI, 2010.

[41] "VisualDOC 6.2 Advanced Examples Manual," Vanderplaats Research and Development, Inc., 2009, pp. 93.

APPENDIX A

SAMPLE LS-DYNA (971 R4) KEYWORD INPUT

Below is a sample keyword input file for LS-DYNA crash simulations. The first keyword file combines different components from separate files. This is done by using the *INCLUDE card and allows a modular and changeable configuration. For example this file defines a translation and then applies this translation to the loadcell wall. The Dodge Neon FE model is then included. Initial velocities are defined for parts in the model and rotational velocities are defined for the wheels. The road surface is defined using a rigid plate with default contact parameters.

```
$# LS-DYNA Keyword file created by LS-PREPOST 2.4 - 19Oct2009(11:13)
$# Created on Feb-18-2010 (14:23:15)
*KEYWORD MEMORY=76385103
*TITLE
$# title
FFI_Steel
*DEFINE_TRANSFORMATION
$---------------------------------------------------------------------------
$#  tranid
     1000
$# option        a1        a2        a3        a4        a5        a6        a7
TRANSL        0.000 160.00000     0.000     0.000     0.000     0.000     0.000
*INCLUDE_TRANSFORM
$# filename
loadcellwall.key
$#  idnoff    ideoff    idpoff    idmoff    idsoff    idfoff    iddoff
         0         0         0         0         0         0         0
$#  idroff
            0
$#  fctmas    fcttim    fctlen    fcttem   incout1
       0.000     0.000     0.000     0.000         0
$#  tranid
     1000
*INCLUDE
$# filename
FFI_neon0.key
*INITIAL_VELOCITY_GENERATION
$#nsid/pid      styp     omega           vx          vy          vz      ivatn
  2000011         3     0.000     15650.000     0.000     0.000         0
$#      xc        yc        zc        nx        ny        nz     phase    iridid
     0.000     0.000     0.000     0.000  1.000000     0.000         0         0
  2000002         1     0.000 15650.000     0.000     0.000         0
     0.000     0.000     0.000     0.000  1.000000     0.000         0         0
  2000003         1 52.200001 15650.000     0.000     0.000         0
 3689.1899     0.000 300.96301     0.000  1.000000     0.000         0         0
  2000004         1 52.200001 15650.000     0.000     0.000         0
 1041.4900     0.000 304.72400     0.000  1.000000     0.000         0         0
*END
```

The second keyword file included is a small portion of the Dodge Neon model used in this study. *CONTROL cards define parameters for various aspects of the model such as general shell and solid element properties. Termination time or length of the simulation is also controlled, 0.15 is the termination time and in the consistent unit set of the model, this is in seconds. *DATABASE cards define the information that will be recorded throughout the simulation. Shown here are output cards for global stats, joint force, material data, node out, and d3plot with the output timestep *dt*. The titles are self explanatory and d3plot is primarily used for visualizing results in a post-processor such as LS-PREPOST. *DATABASE_NODE_HISTORY tells LS-DYNA which nodes to output at intervals specified in nodout.

A *CONTACT definition card is shown next. *CONTACT_AUTOMATIC_SINGLE SURFACE is a general contact type used for most part interactions in this model. A *PART card and its associated cards are shown last. This card defines properties of a part number to which elements are assigned. The part material card is shown for one of the design variable parts used in this study. Shell element material properties are defined here including thickness (T1, T2, T3, and T4).

```
$# LS-DYNA Keyword file created by LS-PREPOST 3.0(Beta) - 19Jan2010(14:34)
$# Created on Mar-29-2010 (13:37:33)
*KEYWORD
*TITLE
$# title
                                LS-DYNA keyword deck by LS-PrePost
$--------------------------------------------------------------------------
$- This model has been developed by the FHWA/NHTSA National Crash Analysis
$- Center at The George Washington University.  The FE model is based on a
$- 1996 Dodge Neon.  The model has been validated to a frontal NCAP test.
$-
$- The model is continuously updated to improve its capabilities in
$- predicting responses in various impact scenarios.  However, the user must
$- verify his own results.  Neither NCAC, GWU, FHWA or NHTSA assume any
$- responsibility for the validity, accuracy, or applicability of any results
$- obtained from this model.
```

```
$- We ask that NCAC be acknowledged under references for any use of this
$- FE model resulting in papers and publications.
$-
$- Please feel free to contact us with any suggestions, comments, or
$- questions.
$-
$-    Dhafer Marzougui      <dmarzoug@ncac.gwu.edu>    (703) 726-8532
$-    Pradeep Mohan         <pradeep@ncac.gwu.edu>     (703) 726-8538
$-    Vinay Nagabhushana    <vinay@ncac.gwu.edu>       (703) 726-8392
$-    Steve Kan             <cdkan@ncac.gwu.edu>       (703) 726-8511
$-
$--------------------------------------------------------------------------------
$- Version 7
$--------------------------------------------------------------------------------
*CONTROL_SHELL
$#  wrpang     esort     irnxx    istupd    theory       bwc     miter      proj
    0.000         1         0         0         0         0         0         0
$# rotascl    intgrd    lamsht    cstyp6    tshell    nfail1    nfail4   psnfail
 1.000000         0         0         1         0         0         0         0
$# psstupd    irquad
        0         0
*CONTROL_SOLID
$#   esort   fmatrix   niptets    swlocl    psfail
        1         0         0         0         0
$#   pm1     pm2     pm3     pm4     pm5     pm6     pm7     pm8     pm9     pm10
      0       0       0       0       0       0       0       0       0       0
*CONTROL_TERMINATION
$#  endtim    endcyc     dtmin    endeng    endmas
 0.150000         0     0.000     0.000     0.000
*CONTROL_TIMESTEP
$#  dtinit    tssfac      isdo    tslimt     dt2ms      lctm     erode     ms1st
    0.000     0.000         0 1.1120E-6 -1.112E-6         0         0         0
$#  dt2msf   dt2mslc     imscl
    0.000         0         0
*DATABASE_GLSTAT
$#      dt    binary      lcur     ioopt
 0.001000         3         0         1
*DATABASE_JNTFORC
$#      dt    binary      lcur     ioopt
 0.001000         3         0         1
*DATABASE_MATSUM
$#      dt    binary      lcur     ioopt
 0.001000         3         0         1
*DATABASE_NODOUT
$#      dt    binary      lcur     ioopt      dthf     binhf
 1.0000E-4         3         0         1     0.000         0
*DATABASE_BINARY_D3PLOT
$#      dt      lcdt      beam     npltc     psetid
 0.005000         0         0         0         0
$#   ioopt
        0
*DATABASE_HISTORY_NODE_SET
$#     id1       id2       id3       id4       id5       id6       id7       id8
  2002000   2002001   2002002   2002003   2002004         0         0         0
*LOAD_BODY_Z
```

```
$#    lcid        sf    lciddr        xc        yc        zc       cid
  2000014  1.000000         0     0.000     0.000     0.000         0
*CONTACT_AUTOMATIC_SINGLE_SURFACE_ID
$#     cid                                                   title
         1
$#    ssid      msid     sstyp     mstyp    sboxid    mboxid       spr       mpr
  2000001         0         2         0         0         0         0         0
$#      fs        fd        dc        vc       vdc    penchk        bt        dt
 0.010000  0.005000     0.000     0.000     0.000         0     0.000     0.000
$#     sfs       sfm       sst       mst      sfst      sfmt       fsf       vsf
    0.000     0.000     0.000     0.000     0.000     0.000     0.000     0.000
$#    soft    sofscl    lcidab    maxpar     sbopt     depth     bsort    frcfrq
         1     0.000         0     0.000     0.000         0         0         0
$# penmax    thkopt    shlthk     snlog     isym     i2d3d    sldthk    sldstf
    0.000         0         0         0         0         0     0.000     0.000
$#    igap    ignore    dprfac    dtstif   unused    unused    flangl
         0         0     0.000     0.000         0         0     0.000
*SET_PART_LIST
$#     sid       da1       da2       da3       da4
  2000001     0.000     0.000     0.000     0.000
$#    pid1      pid2      pid3      pid4      pid5      pid6      pid7      pid8
  2000154   2000161   2000162   2000172   2000173   2000177   2000178   2000179
  2000180   2000181   2000183   2000185   2000186   2000187   2000196   2000197
  2000198   2000199   2000200   2000201   2000202   2000203   2000204   2000205
           [.....]
*PART
$--------------------------------------------------------------------------------
$# title
                                                 CH-A-PILLAR-B-O-L
$#     pid     secid       mid     eosid      hgid      grav    adpopt      tmid
  2000310   2000310   2000310         0         0         0         0         0
*SECTION_SHELL
$#   secid    elform      shrf       nip     propt   qr/irid     icomp     setyp
  2000310        16     0.000         3         1         0         0         1
$#      t1        t2        t3        t4      nloc     marea      idof    edgset
 1.611000  1.611000  1.611000  1.611000     0.000     0.000     0.000         0
*MAT_PIECEWISE_LINEAR_PLASTICITY
$#     mid        ro         e        pr      sigy      etan      fail      tdel
  2000310 7.8900E-9 2.1000E+5  0.300000 330.00000     0.000     0.000     0.000
$#       c         p      lcss      lcsr        vp
 80.000000  4.500000   2000007         0     0.000
$#    eps1      eps2      eps3      eps4      eps5      eps6      eps7      eps8
    0.000     0.000     0.000     0.000     0.000     0.000     0.000     0.000
$#     es1       es2       es3       es4       es5       es6       es7       es8
    0.000     0.000     0.000     0.000     0.000     0.000     0.000     0.000
```

APPENDIX B

SAMPLE MATLAB[7.8] CODES FOR METAMODEL TUNING

This MATLAB script tunes metamodel parameters and uses the tuned models to build an optimized ensemble with them. A cross-validation GMSE and cross-validation average (percent) error for the candidate parameter combinations are calculated. Parameter lists defined by the user are parametrically combined to test all possible combinations of the input parameters. This can become computationally expensive and a type of error minimizations is suggested to enhance parameter tuning. Below is a portion of the code for tuning the RBF values. Other metamodels are similar but may have more or fewer "for" loops depending on the number of parameters. The metamodel functions themselves begin with y_pred_[model name]. The PRS, RBF, and Optimized Ensemble codes are shown following the tuning code portion. GP, KR, and SVR toolboxes developed by Rasmussen and Williams[25] , Lophaven et al.[26] , and Gunn[27] , respectively. In the code below, the DOE points and responses are imported into matrices "dsgnvar" and "y", respectively.

```
% Determine: N = number of DOE points, Ndv = number of design
variables,
% res = number of responses, and Nm = number of metamodels used in the
% ensemble.
N = size(dsgnvar,1);
Ndv = size(dsgnvar,2);
res = size(y,2);
Nm = 5;

% Normalize each design variable to a range of 0 to 1
x_norm = dsgnvar./(ones(N,1)*(max(dsgnvar,[],1)));

%%%%% Begin Metamodel Tuning %%%%

%%% Tune Radial Basis Function (RBF) %%%%
i = 0;
% parameters are choice = radial basis function and c = constant param.
for choice = 1:4         % baseline = 3(multiquadric)
    for c = 0.05:0.05:1; % baseline = 1
        i = i + 1;
        % creating cross-validation Metamodels
        for k = 1:N
            x_in = x_norm;
```

```
            y_in = y;
            x_in(k,:) = [];
            y_in(k,:) = [];
            for r = 1:res
               y_rbf(k,r)=get_ypred_rbfA(x_in,y_in(:,r),x_norm(k,:),...
                Ndv,c,choice);
            end
        end
        %calculating error
        diffRBF = y - y_rbf;
        avg_err_rbf(i,:) = sum(abs(diffRBF).*100./y)./N;
        gmse_rbf(i,:) = sum(diffRBF.^2)./N;
        tune_param_rbf(i,1) = choice;
        tune_param_rbf(i,2) = c;
    end
end
% Finding RBF paramters with lowest average error and GMSE.
[aeRBF,IRBF] = min(avg_err_rbf);
[gmRBF,IRBFg] = min(gmse_rbf);
param_min_rbf(1,:) = tune_param_rbf(IRBF,1)';
param_min_rbf(2,:) = tune_param_rbf(IRBF,2)';
param_min_rbfg(1,:) = tune_param_rbf(IRBFg,1)';
param_min_rbfg(2,:) = tune_param_rbf(IRBFg,2)';

% creating metamodel responses for ensemble using tuned parameters
for k = 1:N
    x_in = x_norm;
    y_in = y;
    x_in(k,:) = [];
    y_in(k,:) = [];
    for r = 1:res
        y_rbf(k,r) = get_ypred_rbfA(x_in,y_in(:,r),x_norm(k,:),...
            Ndv,param_min_rbf(2,r),param_min_rbf(1,r));
        y_rbfg(k,r) = get_ypred_rbfA(x_in,y_in(:,r),x_norm(k,:),...
            Ndv,param_min_rbfg(2,r),param_min_rbfg(1,r));
    end
end

%initializing
y_pred_ens = ones(N,Nm,res); y_pred_ensg = ones(N,Nm,res);
% collecint tuning parameters for each response
param_ens = [param_min_prs; param_min_rbf(2,:);...
    param_min_rbf(1,:); param_min_kr(2,:); param_min_kr(1,:);...
    param_min_kr(3,:);param_min_kr(4,:);param_min_svr(1,:);...
    param_min_svr(2,:);param_min_svr(3,:);param_min_svr(4,:)];
param_ensg = [param_min_prsg; param_min_rbfg(2,:);...
    param_min_rbfg(1,:); param_min_krg(2,:);...
    param_min_krg(1,:);param_min_krg(3,:);...
    param_min_krg(4,:);param_min_svrg(1,:); ...
    param_min_svrg(2,:);param_min_svrg(3,:);param_min_svrg(4,:)];

% creating a 3-D matrix to store metamodel predictions at each DOE
point
% for each response.
y_pred_ensall(:,1,:) = reshape(y_prs,N,1,res);
```

```
y_pred_ensall(:,2,:) = reshape(y_gp,N,1,res);
y_pred_ensall(:,3,:) = reshape(y_rbf,N,1,res);
y_pred_ensall(:,4,:) = reshape(y_krig,N,1,res);
y_pred_ensall(:,5,:) = reshape(y_svr,N,1,res);

y_pred_ensallg(:,1,:) = reshape(y_prsg,N,1,res);
y_pred_ensallg(:,2,:) = reshape(y_gp,N,1,res);
y_pred_ensallg(:,3,:) = reshape(y_rbfg,N,1,res);
y_pred_ensallg(:,4,:) = reshape(y_krigg,N,1,res);
y_pred_ensallg(:,5,:) = reshape(y_svrg,N,1,res);

w_v = zeros(res,Nm);
w_vg = zeros(res,Nm);
% determine the weight factors and ensemble predictions for each
response
for kk = 1:res
    y_pred = y_pred_ensall(:,:,kk);
    y_in = y(:,kk);
    [y_ens(:,kk),w_v(kk,:)] = ensemble_valid(y_in,y_pred);
    y_predg = y_pred_ensallg(:,:,kk);
    [y_ensg(:,kk),w_vg(kk,:)] = ensemble_validg(y_in,y_predg);
end

% Calculate Ensemble Error
diff_ens = y - y_ens;
diff_ensg = y - y_ensg;
avg_err_ens = sum(abs(diff_ens).*100./y)./N;
gmse_ens = sum(diff_ensg.^2)./N;

% Collect Errors for each metamodel
avg_err_all = [aeprs; avg_err_gp; aeRBF; aeKR; aeSVR; avg_err_ens];
gmse_all = [gmprs; gmse_gp; gmRBF; gmKR;gmSVR; gmse_ens];

% Save and write results
save tunemetamodel_MGall_May30
csvwrite('MG_bestparam_ae_5-30.csv', [param_ens;w_v'])
csvwrite('MG_bestparam_gm_5-30.csv', [param_ensg;w_vg'])
```

RBF metamodel…

```
function [y_pred,lambda] = get_ypred_rbf(x,y,x_test,nvar,c,choice)

%x is training points, y is function value at training points, x_test
is test or prediction point, nvar is number of design variables
% choice: 1=thin-plate, 2=gaussian, 3=multiquadric, 4=inverse
multiquadric, 5=inverse multiquadric sqrt

 % c: constant used in RBF formulation

n = size(x,1);  % training
n_test = size(x_test,1);  % test

% Define matrix A
```

```
for i=1:n
    for j=1:n
        xj=x(j,:);
        xi=x(i,:);
        r=norm(xj-xi);
        phi = get_phi(r,c,choice);
        A(i,j) = phi;
    end
end

% Solve for lambda
lambda = A\y;

% Calculate the error at test points
for j = 1:n_test
    y_pred(j,1) = 0;
    xj = x_test(j,:);
    for i = 1:n
        xi = x(i,:);
        r = norm(xj-xi);
        phi = get_phi(r,c,choice);
        y_pred(j,1)=y_pred(j,1)+lambda(i)*phi;
    end
end


%%%%%%%%%%%%%%%%%%%%%%%%%%%%%%%%%%%%%%%%%%%%%%%%%%%%%%%%%%%%%%%%%%%%%%%%%%%%%%%%
%%%%%
function phi = get_phi(r,c,choice)
% choice: 1=thin-plate, 2=gaussian, 3=multiquadric, 4=inverse
multiquadric
if choice == 1
    if r==0
        phi = 0;
    else
        phi = r^2*log(c*r^2);
    end
elseif choice == 2
    phi = exp(-c*r^2);
elseif choice == 3
    phi = sqrt(r^2+c^2);
elseif choice == 4
    phi = 1/sqrt(r^2+c^2);
elseif choice == 5
    phi = c*r;
elseif choice == 6
    phi = (c+r)^3;
end
%%%%%%%%%%%%%%%%%%%%%%%%%%%%%%%%%%%%%%%%%%%%%%%%%%%%%%%%%%%%%%%%%%%%%%%%%%%%%%%%
%%%%%
```

PRS metamodel…

```
function y_pred = get_ypred_prs(x,y,x_test,nvar,npoly)
```

```
%x is training points, y is function value at training points, x_test
is test or prediction point, nvar is number of design variables

% npoly is degree of the polynomial

[X, nbeta1] = create_X_matrix(x, nvar, npoly);
b = X\y;   % solve for the coefficients

% now make predictions
[Xt, nbeta1] = create_X_matrix(x_test, nvar, npoly);
y_pred = Xt*b;

% Create X matrix
function [X, nbeta1] = create_X_matrix(vrn, nvar, npoly)
n_term = 1;
n_beta(1) = 1;
for i=1:10
    n_term = n_term*(nvar+i); %Number of terms in the response surface
for nvar variable problem
    n_beta(i+1) = n_term/factorial(i);
end
nbeta1 = n_beta(npoly+1);

[ndata,n] = size(vrn);

%Create X
X(:,1) = ones(ndata,1);
X = [X vrn];
X1 = vrn;
nc1 = nvar;
n_loc = [1:nvar];
n_loc1 = 1;
for i = 2:npoly
    [nr,nc]=size(X1);
    clear X2;
    ctr=1;
    for k=1:nvar
        l_ctr = 0;
        for j=n_loc(k):nc
            X2(:,ctr) = vrn(:,k).*X1(:,j);
            ctr = ctr+1;
            l_ctr = l_ctr+1;
        end
        n_loc1(k+1)=l_ctr + n_loc1(k);
    end
    nc1 = nc;
    X = [X X2];
    X1 = X2;
    n_loc = n_loc1;
end
```